Plate finite elements with arbitrary displacement fields along the thickness

Finite Elements in Analysis and Design 244 (2025) 104296

Contents lists available at ScienceDirect

Finite Elements in Analysis & Design

journal homepage: www.elsevier.com/locate/finel

Plate finite elements with arbitrary displacement fields along the thickness

E. Carrera [a,b,1], D. Scano [a,*,2], E. Zappino [a,3]

[a] MUL2 Lab, Department of Mechanical and Aerospace Engineering, Politecnico di Torino, Corso Duca degli Abruzzi 24, 10129 Torino, Italy
[b] Department of Mechanical Engineering, College of Engineering, Prince Mohammad Bin Fahd University, P.O. Box 1664, Al Khobar 31952, Kingdom of Saudi Arabia

ARTICLE INFO

Keywords:
Finite element method
Plate models
Carrera Unified Formulation
Refined theories
Taylor polynomials

ABSTRACT

The present paper introduces a methodology for formulating two-dimensional structural theories featuring arbitrary kinematic fields. In the proposed approach, each displacement variable can be examined through an independent expansion function, enabling the integration of both classical and higher-order theories within a unified framework. The Carrera Unified Formulation is used to derive the governing equations in a unified form, independent of the expansion adopted for each displacement component. In this paper, plate structural theories are constructed by using polynomial expansions. The finite element method is used to discretize the structure in the reference plane of the plate, utilizing Lagrange-based elements. The Mixed Interpolation of Tensorial Components is adopted to alleviate the shear locking issues. In this study, isotropic plate structures are investigated under various loadings, boundary conditions, and different length-to-thickness ratios. Whenever possible, the present results are compared with analytical and literature solutions. The accuracy of the presented models is evaluated for both displacements and stress components. The findings indicate that the selection of the most appropriate model is strongly dependent on the specific parameters of the individual problem, however, choosing the right model can significantly enhance the efficiency of the numerical analysis.

1. Introduction

Modern advanced engineering fields, ranging from industrial applications to bio-mechanics, eventually requires complicated and computationally expensive structural analyses. Appropriate two-dimensional (2D) models can be adopted to analyse the three-dimensional (3D) continuum for some geometries and to reduce the required computer power. Despite advancements in computational mechanics and computing power, plate models remain popular due to their relative simplicity. In fact, 2D models can capture essential aspects of structural behaviour. These models find extensive applications in engineering, e.g., aircraft panels and helicopter rotor blades in aerospace engineering.

In recent years, researchers have made significant progress in accurately predicting specific structural behaviours while striving to balance accuracy and computational efficiency using various plate models. One of the most critical issue is that the researchers

* Corresponding author.
E-mail addresses: erasmo.carrera@polito.it (E. Carrera), daniele.scano@polito.it (D. Scano), enrico.zappino@polito.it (E. Zappino).
[1] Professor of Aeronautics and Astronautics.
[2] Ph.D. Student.
[3] Associate Professor.

https://doi.org/10.1016/j.finel.2024.104296
Received 17 September 2024; Received in revised form 21 November 2024; Accepted 4 December 2024
Available online 14 December 2024

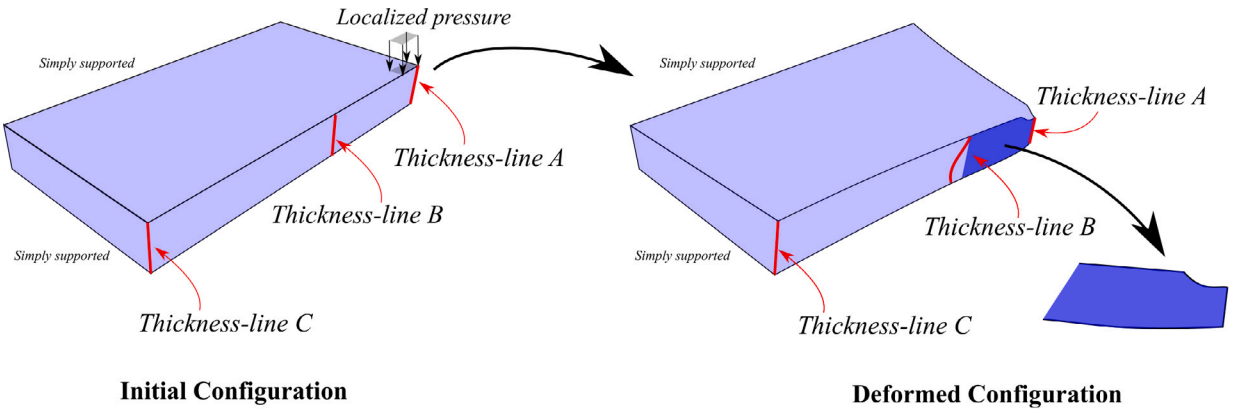

Fig. 1. Localized deformations on different thickness-lines of a plate structure.

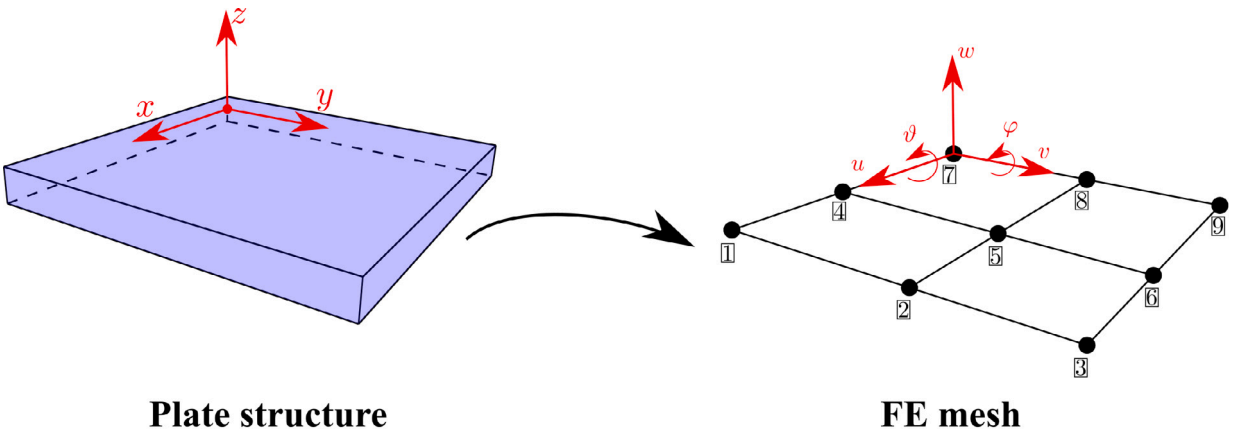

Fig. 2. Classical two-dimensional finite elements.

have to redefine a new theory and recalculate the governing equations every time. This paper introduces a general method that addresses this issue for the plate formulation by creating a framework that enables the generation of any structural theory. The aim of this work is to provide a consistent formulation that allows users to select the desired theory and accuracy level.

The thickness-wise deformation of plates. Structures generally undergo deformation due to various conditions, such as types of loads, materials, boundary conditions, geometrical properties, and many others that can arise in specific cases [1]. Deformation pattern depends on the specific problem under consideration and on the considered position of the structure. Fig. 1 depicts a plate loaded by a localized pressure with two simply-supported edges. The initial and deformed configurations are shown. In particular, three thickness-lines are taken into account. The load significantly affects Thickness-lines A and B, causing noticeable deformations and pinching near Thickness-line A, while Thickness-line C, close to a clamped edge, is slightly affected. That is, *assigning the same degree of freedom to all three thickness-lines would be inefficient.* This aspect is particularly evident in the laminated structures, where complicated phenomena arise. See [2] for more information.

Classical and Refined plate approaches. Several plate models have been proposed, with Thin Plate Theory (TPT) standing out as a classical model. TPT relies on Kirchhoff's hypotheses [3], which exclude transverse shear and through-the-thickness deformation. The inclusion of transverse shear deformation in TPT leads to the Reissner–Mindlin theory [4,5], commonly referred to as the First-Order Shear Deformation Theory (FSDT). While classical theories are suitable primarily for isotropic and thin cases, they were predominant in the early Finite Element Method (FEM) plate formulations, as exemplified in Argyris [6]. Many plate elements are grounded in Lagrange polynomials. For instance, Pryor and Barker [7] introduced a four-node element to investigate transverse shear effects. Leonetti and Aristodemo [8] implemented a mixed finite element model to study linear and plastic collapse plane problems. Ribaric and Jelenic [9] used a higher-order FE based on the FSDT to study thick plates. Classical models continue to be employed in contemporary commercial codes. To this end, Fig. 2 illustrates a plate structure discretized with classical four-node 2D elements. Three displacements and two rotations are the unknowns for each FE node, i.e., only five Degrees Of Freedom (DOF) per each node. A detailed explanation of various classical elements can be found in Bathe [10].

Classical plate elements face limitations in accurately capturing local effects and nonlinear deformations, particularly in the analysis of thicker plates. A more effective approach involves the use of 3D elements (as discussed by Argyris [11]). In particular,

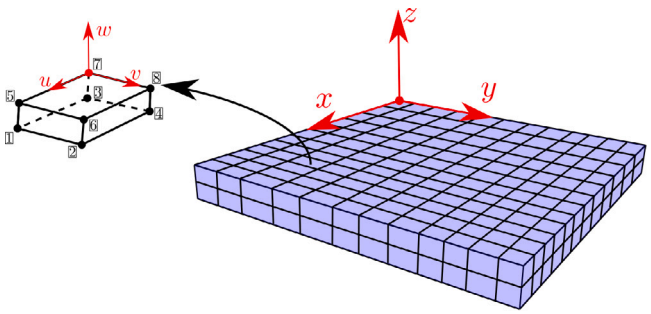

Fig. 3. Use of three-dimensional finite elements to discretize a plate-like structure.

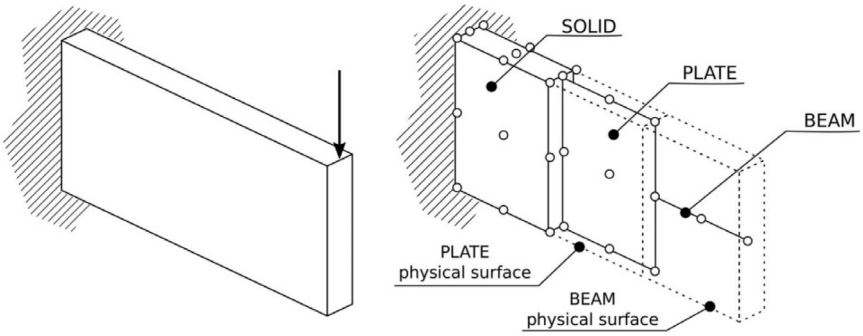

Fig. 4. Use of a global–local method to discretize a structure, reported from Zappino and Carrera [1].

each FE node is described by only three displacements , as shown in Fig. 3 for a plate-like structure. Combining 3D and 2D FE elements is also a viable approach, as demonstrated by Surana [12,13]. Dávila [14] proposed two methods to combine solid and plate models — one based on the FSDT assumptions, and another on a higher-order theory. Blanco et al. [15] coupled incompatible 3D and 2D models under the Naghdi hypothesis. Zappino and Carrera [1] introduced an approach to unify 1D, 2D, and 3D models within a single formulation reducing computational costs and enhancing efficiency. Several global/local methods have been employed, as discussed by Noor [16]. Fig. 4 pictorially describes the possibility to integrate the three formulations.

However, also several refined plate models have been proposed. First, the so-called axiomatic theories are briefly reviewed, where scientists made assumptions for the behaviour of structures. Advanced 2D models have been developed to overcome the limitations of classical plate theories. For instance, see Reddy's influential book [17]. Comprehensive reviews of advanced plate models can be found in the works of Reddy and Robbins [18] and Carrera [19]. Additional insights into higher-order plate theories were provided by Washizu [20]. The general theory can be written in the following expansion:

$$\begin{aligned} u_x &= u_{x_1} + zu_{x_2} + z^2u_{x_3} + \cdots + z^{N-1}u_{x_N} \\ u_y &= u_{y_1} + zu_{y_2} + z^2u_{y_3} + \cdots + z^{N-1}u_{y_N} \\ u_z &= u_{z_1} + xu_{z_2} + z^2u_{z_3} + \cdots + z^{N-1}u_{z_N} \end{aligned} \tag{1}$$

In these theories, higher-order expansions of the displacement variables are assumed along the thickness of the structure and were presented by Kant et al. [21] and Kant and Kommineni [22]. Reddy [23] employed refined models for plates structures. Swaminathan and Patil [24] presented an analytical solution with twelve degrees of degrees for dynamic analysis. Kant and Swaminathan [25] compared five classical and refined theories from literature: (a) Kant and Majunatha [26], (b) Pandya and Kant [27], (c) Reddy [28], (d) Senthilnathan et al. [29], and (e) Whitney and Pagano [30].

The Carrera Unified Formulation vs axiomatic and asymptotic approaches. At last, Carrera and Demasi [2] proposed the Carrera Unified Formulation (CUF) for plate theories. CUF has been applied also to the beam formulation, see Carrera et al. [31]. Thanks to this method, it is possible to choose the structural theory and the shape functions over the mid-plane freely. CUF has been used in several applications. CUF was also used for thermal applications (see for example Robaldo et al. [32]), and multilayered plates embedding piezo-layers were studied by Ballhause et al. [33]. Many other papers study multilayered plates and shells by using CUF. The interested reader can refer to Carrera [34] for more details and references. Concerning the shape functions, several elements have been proposed in the CUF literature, ranging from the classical four-node to the higher-order nine- and sixteen-node Lagrange-based elements. Also, hierarchical FE have been assessed, see [35].

In addition to axiomatic theories, it is possible to define the asymptotic methods. These approaches [36,37] begin with the 3D equations, identifying a perturbation parameter δ (often the length-to-thickness ratio), and derive theories associated with the

Table 1
Complete fourth-order Taylor theory, Number of Terms = 15. All the terms are indicated by the black bullets.

Variable	1	z	z^2	z^3	z^4
u_x	•	•	•	•	•
u_y	•	•	•	•	•
u_z	•	•	•	•	•

Table 2
Reduced fourth-order Taylor theory, Number of Terms = 10. The black bullets indicate the considered terms, while the empty circles stand for the disregarded terms.

Variable	1	z	z^2	z^3	z^4
u_x	•	∘	•	∘	•
u_y	∘	∘	•	•	•
u_z	•	•	∘	•	•

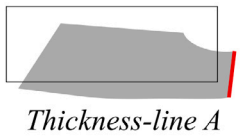

Variable	1	z	z^2	z^3	z^4
u_x	●	●	○	○	○
u_y	●	●	○	○	○
u_z	●	○	●	●	○

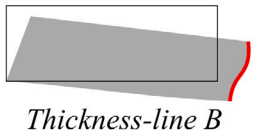

Variable	1	z	z^2	z^3	z^4
u_x	●	●	●	○	●
u_y	●	●	○	○	●
u_z	●	●	○	○	○

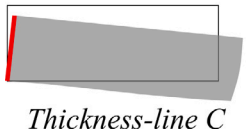

Variable	1	z	z^2	z^3	z^4
u_x	●	●	○	○	○
u_y	●	●	○	○	○
u_z	●	●	○	○	○

Fig. 5. Use of different reduced models for the study of tree thickness-lines from Fig. 1.

same order in δ. This approach offers a direct estimation of solution accuracy compared to the exact 3D solution. However, many parameters should be used to deal with thick structures and intricate phenomena. For example, Aghalovyan and Aghalovyan [38] investigated thermoelastic and dynamic problems in thin structures, while Berdichevsky [39] proposed an asymptotic method for studying sandwich plates. *Aim of the present paper.* The primary objective of this work is to develop a method for assessing the meaning of individual terms within an expansion. In structural analysis, computational efficiency is crucial. Thus, the aim is to achieve reliable results with minimal computational cost, which is of significant interest. The ultimate goal is to construct the most advantageous models, specifically reduced models, while ensuring the desired level of accuracy.

The generation of reduced theories may be effectively illustrated, as in Tables 1 and 2, where each displacement variable is represented by polynomial terms. The black bullets reveal the presence of the terms, while the empty circles denote their absence. Table 1 presents a complete fourth-order Taylor theory with fifteen terms. However, it is essential to examine the impact of individual terms. Table 2 provides an illustration of a fourth-order model with only ten terms included, balancing accuracy with reduced complexity. Reminding the example of Fig. 1, Fig. 5 illustrates the three thickness-lines of the plate, allowing specific models for a detailed deformation analysis. For instance, for the analysis of Thickness-line B, the most refined model with nine terms could be efficiently employed. Thickness-line A highlights the importance of higher-order terms in transverse displacement for accurate deformed representation.

From the previous considerations, the Asymptotic-Axiomatic Method (AAM) has been presented. See, for instance, [40]. As the name suggests, it is possible to unify the capabilities of the two philosophies. In particular, the AAM starts from the definition of a complete axiomatic theory (e.g., TE4 as in Table 1) and then the role of each term can be studied considering several parameters such as loading and boundary conditions, materials or length-to-thickness ratios. This method consists of various steps: (a) the problem data – e.g., BCs, materials and other characteristics of the structure – must be identified; (b) the output variable are calculated, such as displacements, stresses, or frequencies; (c) a starting complete theory is selected and often regarded as the reference model

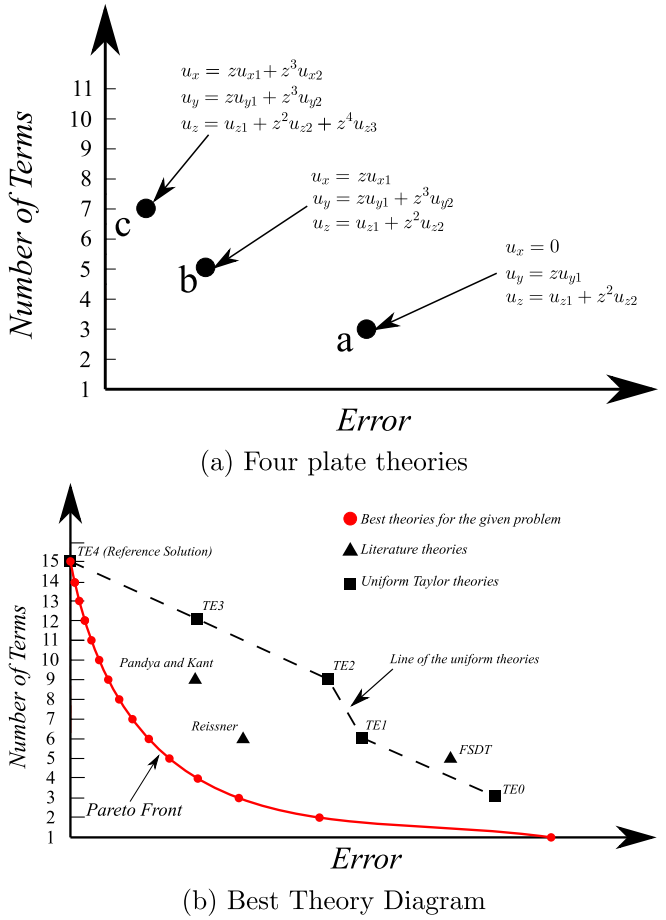

Fig. 6. Example of a 2D plot Error-Number of Terms (a) and a Best Theory Diagram (b).

because it aims to provide a solution that closely resembles the behaviour of the actual 3D system; (d) then it is possible to choose a reduced theory, that is, the terms considered for the displacement variables are established; (e) the derived governing equations are using the CUF, even though other formulations could be employed; (f) the accuracy of the theory is typically assessed by comparing its results with those obtained from a reference solution.

From this process it is possible to build a two-dimensional graph, see Fig. 6(a). On the horizontal axis lays the error calculated respect to a reference theory. The number of considered terms is indicated on the y-axis. This graph is useful to immediately understand the capabilities of a theory for a given problem. The final result of the process of analysing all the theories up to a determined order is the Best Theory Diagram (BTD), see Fig. 6(b). This curve (i.e., a Pareto front) is composed by all the models with the least error for a given number of terms. In this example, the complete fourth-order model (TE4) serves as the reference solution. This is not a strict rule, because also 3D and analytical solutions, if available, can be chosen. Additionally, uniform theories can be represented where all three displacement variables adopt the same complete expansion. The literature models can be inserted in the graph as well. In Fig. 6(b) the following models are used as examples: FSDT [4,5], Reissner [41], Pandya and Kant [27]. It is important to note that the diagram depends on the analysed problem and the desired output.

The development of a unified method for automatically generating reduced plate models, similar to those illustrated in Table 2, remains an area of ongoing research in the literature. A preliminary work has been presented by Carrera et al. [42] for the beam formulation within the CUF framework. Such a unified method is essential for achieving the most efficient computational model, as it allows for the reduction of the number of degrees of freedom while maintaining a predefined level of accuracy. In recent years, several studies within the context of CUF have focused on understanding the significance of different terms in displacement variables Carrera and co-authors [43–45] examined the efficacy of terms in Taylor-based expansions within the plate formulation for the displacement and stresses. Also, frequencies in dynamic responses have been considered as the control parameters. Higher-order nine-node Lagrange finite elements were used over the mid-plane of the structure. In particular, a penalization technique for the stiffness matrix is used to simulate the elimination of the terms. However, the stiffness matrix has always the dimension of the most

Table 3
Acronyms used in the present paper.

Acronym	Meaning
CUF	Carrera Unified Formulation
TE	Taylor Expansion
TPT	Thin Plate Theory
FSDT	First-order Shear Deformation Theory
HOT	Higher-Order Theories
DOF	Degrees of Freedom
MITC	Mixed Interpolation of Tensorial Components
Q9	Square nine-noded Lagrange element
FE	Finite Element
FEM	Finite Element Method
FN	Fundamental Nucleus
AAM	Asymptotic-Axiomatic Method
BTD	Best Theory Diagram
NDK	Node Dependent Kinematics

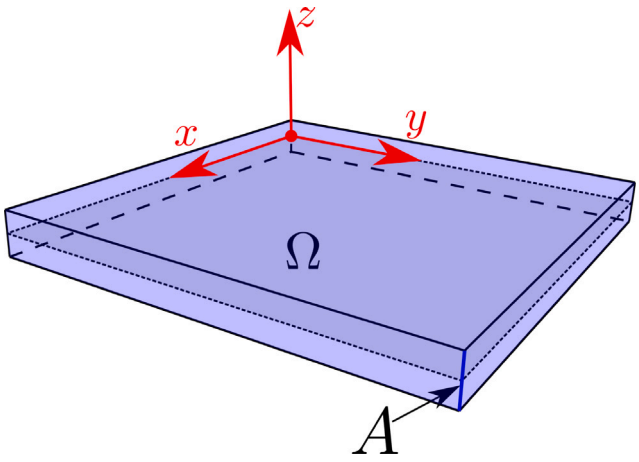

Fig. 7. Reference system for a generic plate-like structure.

accurate theory. For example, considering the Table 1 once more, all the analyses actually have 15 terms for each FE node, from a computational point of view. In contrast, Demasi [46] introduced the Generalized Unified Formulation (GUF) for analising plate structures for closed-form solution. Then, the GUF was extended by the same author [47] to a two-dimensional FE framework. In this approach, the 3×3 Fundamental Nucleus (FN) of the stiffness matrix is replaced by a scalar FN. This reformulation allows for the reordering of the global stiffness matrix, facilitating the independent definition of displacements.

This works introduces a method to employ models similar to that described in Eq. (1), within the framework of CUF. The method is designed to be adaptable to various theories, and its utility is demonstrated in Table 2. The goal of this work is to redefine the Unified formulation to simplify the development of specialized plate theories within the FE method. Essentially, the previous version of the unified formulation used a 3×3 FN $\mathbf{K}$ (3 stands for the number of displacement components). Since there is a single submatrix, it is not possible to decide the expansion for each component. The only way to delete some terms was to adopt some ad-hoc penalization techniques, as in [43]. These limitations have led to a change in the paradigm of the unified formulation. In particular, the concept of the submatrix 3×3 has been substituted by the scalar FN K. This allows complete freedom in choosing the theories and the number of terms. In the new method, it is also possible to delete the contribution of one or more displacement components as in the cylindrical bending conditions. Now, the dimensions of the structural matrices are more tailored with respect to the 'classical' CUF. By employing the new approach, the stiffness matrix can maintain consistent dimensions, ensuring compatibility with different kinematic models. For the sake of clarity, the details of the new assembly process is given in Section 4.3.

The paper primarily focuses on analysing isotropic structures. Overall, the work aims to enhance the development of specialized plate theories within FE analysis and lays the groundwork for future exploration of the AAM methodology.

FE analysis may encounter notable stiffening issues, particularly with thin structures. Shear locking impacts plate elements, where FEs struggle to accurately calculate bending deformation, mistakenly channelling strain energy into shear modes. One of the most effective approaches is the Mixed Interpolation of Tensorial Components (MITC) method [48,49]. Cinefra and Carrera [50] first included this integration scheme in the CUF framework.

This paper is organized as follows: (a) In Section 2, various plate theories from the literature are presented, along with illustrations of Taylor-based expansions and an explanation of the concept of reduced theories. (b) Section 3 outlines the principles of the Unified formulation approximation and its integration with the finite element method. (c) Section 4 derives the governing equations by

adopting the principle of virtual displacements. (d) Section 5 show an example for the assembly of the stiffness matrix and load vector. (e) Results for displacements and stresses are presented in Section 6. (f) Finally, the main conclusions are summarized in Section 7.

For the list ofsee Table 3

2. Review of the plate theories

Fig. 7 depicts a generic isotropic and a Cartesian reference system. The Thickness-line A is placed along the thickness direction z. Instead, the mid-plane Ω is located in the x–y plane of the structure. The three-dimensional displacement field is the following:

$$\mathbf{u}(x,y,z) = \left\{ \begin{array}{ccc} u_x(x,y,z), & u_y(x,y,z), & u_z(x,y,z) \end{array} \right\}^T \tag{2}$$

The brief review in Section 1 shows how scientists have proposed many models. In particular, each component of the displacement variable, i.e., u_x, u_y, and u_z can be studied with different expansions.

To this end, the present section explicitly presents several theories, ranging from the classical to more advanced higher-order models. Some have been briefly presented in the Introduction.

2.1. Classical plate theories

First, one of the simplest models is the Membrane Theory (see Carrera et al. [51]) where only the three constant terms are considered:

$$\begin{array}{lcl} u_x(x,y,z) & = & u_{x_1}(x,y) \\ u_y(x,y,z) & = & u_{y_1}(x,y) \\ u_z(x,y,z) & = & u_{z_1}(x,y) \end{array} \tag{3}$$

Second, the displacement field of the Thin Plate Theory (TPT) is slightly more complex, see [3]. The three variables are described as follows:

$$\begin{array}{lcl} u_x(x,y,z) & = & u_{x_1}(x,y) - \frac{\partial u_{z_1}(x,y)}{\partial x} z \\ u_y(x,y,z) & = & u_{y_1}(x,y) - \frac{\partial u_{z_1}(x,y)}{\partial y} z \\ u_z(x,y,z) & = & u_{z_1}(x,y) \end{array} \tag{4}$$

Third, the First-order Shear Deformation Theory (FSDT) uses five term, see [4,5] for more details. The displacement field is written in the following:

$$\begin{array}{lcl} u_x(x,y,z) & = & u_{x_1}(x,y) + \phi_y(x,y) z \\ u_y(x,y,z) & = & u_{y_1}(x,y) + \phi_x(x,y) z \\ u_z(x,y,z) & = & u_{z_1}(x,y) \end{array} \tag{5}$$

In these models, u_{x_1}, u_{y_1}, and u_{z_1} denote the displacements of the plate's reference mid-surface in the x, y, and z directions, respectively. The terms ϕ_y and ϕ_x represent the rotations about y and x axes. Conversely, the factors $-\frac{\partial u_{z_1}(x,y)}{\partial x}$ and $-\frac{\partial u_{z_1}(x,y)}{\partial y}$ describe rotations about y and x axes, if the shear deformation is not considered. Fig. 8 visually depicts these classical theories in the $y-z$ and $x-z$ planes for the sake of clarity.

2.2. Use of ad-hoc higher-order theories

After having explored the mathematical formulation of three widely used classical theories, the attention is here focussed on some Higher-Order Theories (HOTs) presented in literature.

As first example, Lo et al. [52] proposed the following model:

$$\begin{array}{l} u_x(x,y,z) = u_{x_0}(x,y) + z\psi_x(x,y) + z^2\zeta_x(x,y) + z^3\phi_x(x,y) \\ u_y(x,y,z) = u_{y_0}(x,y) + z\psi_y(x,y) + z^2\zeta_y(x,y) + z^3\phi_y(x,y) \\ u_z(x,y,z) = u_{z_0}(x,y) + z\psi_z(x,y) + z^2\zeta_z(x,y) \end{array} \tag{6}$$

On the other hand, Reissner [41] presented an interesting theory where some terms of the previous equations are disregarded.

$$\begin{array}{l} u_x(x,y,z) = z\psi_x(x,y) + z^3\phi_x(x,y) \\ u_y(x,y,z) = z\psi_y(x,y) + z^3\phi_y(x,y) \\ u_z(x,y,z) = u_{z_0}(x,y) + z^2\zeta_z(x,y) \end{array} \tag{7}$$

When focusing on specific loading cases, such as cylindrical bending, it is possible to use simplifying hypotheses. To this end, the influence of the y direction is entirely disregarded. Consequently, also the variable u_y is omitted. For instance, Manjunatha and Kant [53] introduced a simplified theory which is given in the following:

$$\begin{array}{l} u_x(x,z) = z\psi_x(x) + z^3\phi_x(x) \\ u_z(x,z) = u_{z_0}(x) + z^2\zeta_z(x) \end{array} \tag{8}$$

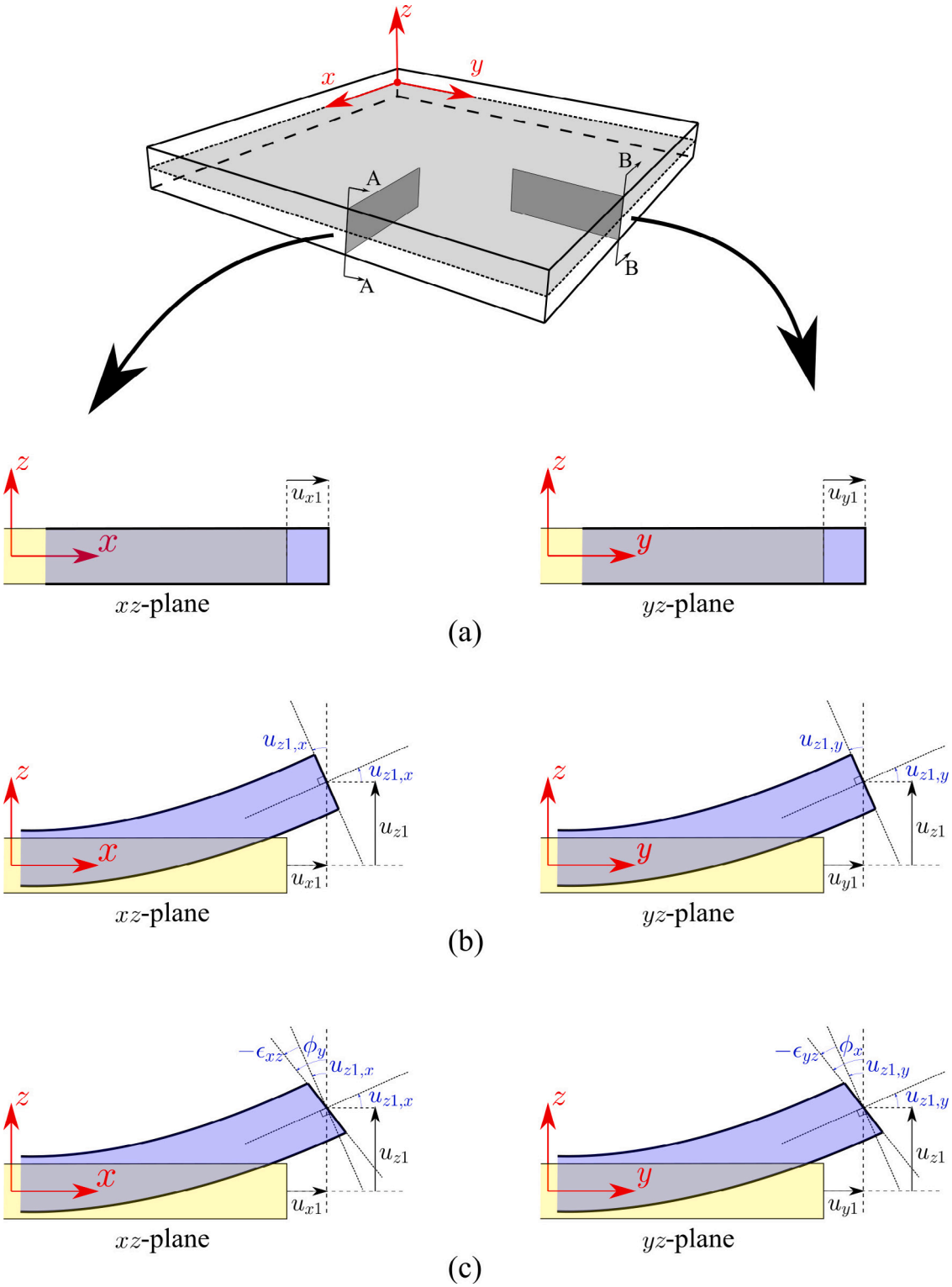

Fig. 8. Differences between classical plate theories: Membrane Theory (a), Thin Plate Theory (b), and First-order Shear Deformation Theory (c).

The preceding examples have demonstrated how scientists endeavoured to formulate customized plate models efficiently for the analysis of various problems. These concepts will be further explored in the subsequent Section 2.3, where Taylor-based models will be discussed.

2.3. Taylor-based higher-order theories

Taylor polynomials of the form z^b, where b is a positive integer, are utilized to develop Higher-Order Theories (HOTs) for analysing plate behaviour. These polynomials are adopted to modelling the responses plate of the thickness-lines in detail. Within the CUF framework, Carrera [19] explored the capabilities of such polynomials for plates, extending from first to fourth orders, thereby enabling the incorporation of higher-order effects more comprehensively.

Uniform theories In the literature on the CUF applied to plate formulations, it is common to assume the same expansion across all three displacement variables. This approach gives rise to what are known as *uniform* theories. For example, a theory of the third order within this context might be described in the following manner:

$$\begin{aligned} u_x &= u_{x_1} + zu_{x_2} + z^2u_{x_3} + z^3u_{x_4} \\ u_y &= u_{y_1} + zu_{y_2} + z^2u_{y_3} + z^3u_{y_4} \\ u_z &= u_{z_1} + zu_{z_2} + z^2u_{z_3} + z^3u_{z_4} \end{aligned} \tag{9}$$

Different theories Previous uniform theories applied the same level of expansion to all displacement variables. Nonetheless, this paper introduces results where u_x, and u_y, and u_z are approximated with varying polynomial orders. For example, the structural theory discussed here utilizes a second-order expansion for u_x and u_z, and a third-order expansion for u_y, demonstrating a tailored approach to modelling the displacement components:

$$\begin{aligned} u_x &= u_{x_1} + zu_{x_2} + z^2u_{x_3} \\ u_y &= u_{y_1} + zu_{y_2} + z^2u_{y_3} + z^3u_{y_4} \\ u_z &= u_{z_1} + zu_{z_2} + z^2u_{z_3} \end{aligned} \tag{10}$$

This theory consists of ten terms, differing from the uniform third-order theory (Eq. (9)), which incorporates twelve expansion functions.

Reduced theories In both *uniform* and *different* theories, comprehensive Taylor expansions are showcased, signifying the inclusion of all terms within each displacement variable. Yet, based on physical insights, it becomes evident that certain terms may be omitted. Consequently, this facilitates the construction of what are termed *reduced theories*, modelled as follows:

$$\begin{aligned} u_x &= u_{x_1} + zu_{x_2} \\ u_y &= u_{y_1} + z^2u_{y_2} + z^3u_{y_3} \\ u_z &= u_{z_1} \end{aligned} \tag{11}$$

Attention is drawn to the differences in the u_y component between Eq. (9) (or Eq. (10)) and Eq. (11). In the initial equations, all four terms are preserved, whereas the latter equation opts to incorporate only three of these terms. Taking into account the variables u_x and u_z as well, the reduced model in Eq. (11) now encompasses a total of six terms, signifying a notable reduction in degrees of freedom compared to the uniform theory. Please note that the subscripts are updated.

In the CUF literature, the elimination of a term is facilitated through a penalization technique, starting from a comprehensive uniform theory. Consequently, the effective number of terms remains constant. For a more detailed explanation, please refer to [51].

3. Unified formulation for plate and generalization to the higher-order theories

In the preceding sections, various models found in the literature have been presented, and it is also feasible to devise new *ad hoc* models. The CUF possesses a unique ability to succinctly describe these models, all stemming from a common mathematical foundation. Within this context, a general variable (such as displacement, stress, or strain component) denoted as f is represented in relation to one or more M additional unknowns $f_\tau(\tau = 1, \dots, M)$. They are defined at a specified point on the plate thickness-line, generally corresponding to the mid-plane of the plate. The expansion is formulated by introducing base functions $F_\tau(z)$ along the plate thickness-line, and this relationship is captured by the following formula:

$$f(x, y, z) = \sum_{\tau=1}^{M} F_\tau(z) f_\tau(x, y) = F_\tau(z) f_\tau(x, y), \qquad \tau = 1, 2, \dots, M \tag{12}$$

In this paper the Einstein's convention will be used for the sake of brevity.

In the present formulation, the components of the 3D displacement field are approximated by arbitrary functions, defined along the thickness-line:

$$u_x = F_{u_x\tau}(z)u_{x_\tau}(x,y) \text{ with } \tau = 1,\dots,M_{u_x}$$
$$u_y = F_{u_y\tau}(z)u_{y_\tau}(x,y) \text{ with } \tau = 1,\dots,M_{u_y} \tag{13}$$
$$u_z = F_{u_z\tau}(z)u_{z_\tau}(x,y) \text{ with } \tau = 1,\dots,M_{u_z}$$

$F_{u_x\tau}$, $F_{u_y\tau}$, and $F_{u_z\tau}$ are the expansion functions for the *generalized* displacements u_{x_τ}, u_{y_τ}, and u_{z_τ}, respectively. In this work, each displacement variable can be discretized by different functions, while in previous CUF-based works [2] the expansions were identical for all three components. The symbol τ denotes summation, while M_{u_x}, M_{u_y}, and M_{u_z} signify the number of expansions for each displacement variable. It is crucial to emphasize that the value of τ varies depending on the specific component under consideration.

It is also possible to write the three virtual displacement variables as follows:

$$\delta u_x = F_{u_x s}(z)\delta u_{x_s}(x,y) \text{ with } s = 1,\dots,M_{u_x}$$
$$\delta u_y = F_{u_y s}(z)\delta u_{y_s}(x,y) \text{ with } s = 1,\dots,M_{u_y} \tag{14}$$
$$\delta u_z = F_{u_z s}(z)\delta u_{z_s}(x,y) \text{ with } s = 1,\dots,M_{u_z}$$

Here, $F_{u_x s}$, $F_{u_y s}$, and $F_{u_z s}$ represent the expansion functions in the virtual system. Notably, the subscript τ is substituted with s.

The CUF approximation and the Finite Element Method (FEM) can be successfully integrated to yield numerical results. FEM is utilized to discretize displacements across the mid-plane. Thence, the displacements are written as in the followings:

$$u_x = N_i(x,y)F_{u_x\tau}(z)q_{x_{\tau i}} \text{ with } \tau = 1,\dots,M_{u_x} \text{ and } i = 1,\dots,N_n$$
$$u_y = N_i(x,y)F_{u_y\tau}(z)q_{y_{\tau i}} \text{ with } \tau = 1,\dots,M_{u_y} \text{ and } i = 1,\dots,N_n \tag{15}$$
$$u_z = N_i(x,y)F_{u_z\tau}(z)q_{z_{\tau i}} \text{ with } \tau = 1,\dots,M_{u_z} \text{ and } i = 1,\dots,N_n$$

while their virtual variations read as:

$$\delta u_x = N_j(x,y)F_{u_x s}(z)\delta q_{x_{sj}} \text{ with } s = 1,\dots,M_{u_x} \text{ and } j = 1,\dots,N_n$$
$$\delta u_y = N_j(x,y)F_{u_y s}(z)\delta q_{y_{sj}} \text{ with } s = 1,\dots,M_{u_y} \text{ and } j = 1,\dots,N_n \tag{16}$$
$$\delta u_z = N_j(x,y)F_{u_z s}(z)\delta q_{z_{sj}} \text{ with } s = 1,\dots,M_{u_z} \text{ and } j = 1,\dots,N_n$$

Here, N_i and N_j represent the shape functions, with the repeated subscripts i and j signifying summation. N_n denotes the number of shape functions per element. In this study, the classical nine-node Lagrange (denoted as Q9) element is employed for numerical assessments. For further details, refer to Bathe [10].

It is convenient to introduce a concise notation for both real and virtual systems, as illustrated below:

$$u_l = N_i F_{u_l\tau} q_{l_{\tau i}} = \sum_{i=1}^{N_n}\sum_{\tau=1}^{M_{u_l}} N_i F_{u_l\tau} q_{l_{\tau i}} \tag{17}$$

$$\delta u_m = N_j F_{u_m s}\delta q_{m_{sj}} = \sum_{j=1}^{N_n}\sum_{s=1}^{M_{u_m}} N_j F_{u_m s}\delta q_{m_{sj}} \tag{18}$$

Here, l and m can assume the values of x, y, and z. In particular, there is no summation over l (or m). This formulation proves advantageous for the assembly of the matrices of the linear structural system, as elaborated in the subsequent Section 4.

4. Governing equations and finite element matrices

The first step in determining the governing equations and the FE matrices is to give the expressions for stress, $\boldsymbol{\sigma}$, and strain, $\boldsymbol{\epsilon}$, tensors. In classical elasticity, their vectorial form can be written as follows:

$$\boldsymbol{\sigma} = \left\{ \begin{array}{cccccc} \sigma_{xx} & \sigma_{yy} & \sigma_{zz} & \sigma_{yz} & \sigma_{xz} & \sigma_{xy} \end{array} \right\}^T \quad \boldsymbol{\epsilon} = \left\{ \begin{array}{cccccc} \epsilon_{xx} & \epsilon_{yy} & \epsilon_{zz} & \epsilon_{yz} & \epsilon_{xz} & \epsilon_{xy} \end{array} \right\}^T \tag{19}$$

The geometrical relations strains-displacements read as:

$$\boldsymbol{\epsilon} = \mathbf{D}\mathbf{u} \tag{20}$$

where $\mathbf{D}$ represents the matrix of differential operators for small displacements and angles of rotation can be found in [51]. This work assumes linear elastic isotropic materials, leading to the following constitutive relation:

$$\boldsymbol{\sigma} = \mathbf{C}\boldsymbol{\epsilon} \tag{21}$$

where the matrix of material coefficients, $\mathbf{C}$ is described in [10].

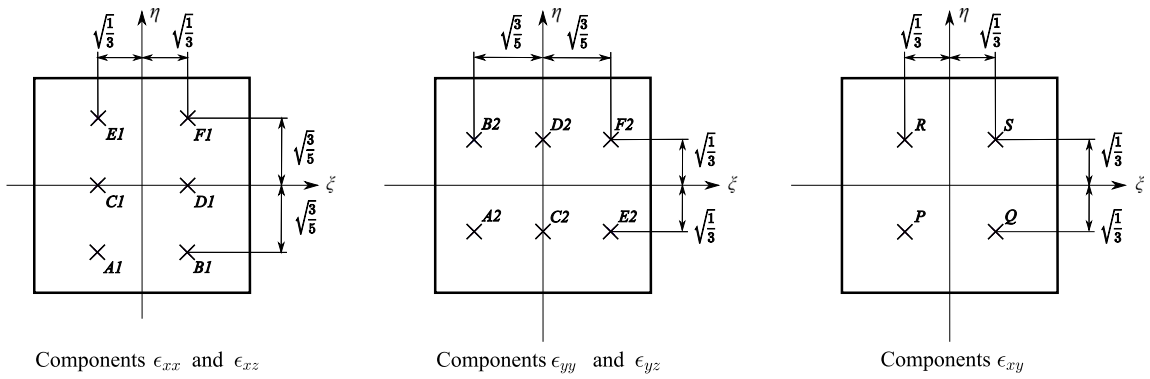

Fig. 9. Tying points for the MITC Q9 plate elements used for different strain components.

4.1. MITC Q9

In this work, however, the Mixed Interpolation of Tensorial Components (MITC) method is adopted to counteract the shear locking issue present in Finite Element (FE) formulations. For more information, see Bathe et al. [54]. The MITC method has been extensively employed in CUF literature [50]. Since Lagrangian nine-node elements are used, the element is usually named MITC Q9. Considering the natural coordinate system (ξ, η), the MITC elements are formulated by employing an interpolation approach. Rather than directly computing the strain components from the displacements, an interpolation of these components is conducted within each element. This involves employing a specific interpolation strategy tailored to each component. Fig. 9 shows the positions of the tying points and their coordinates in the $\xi-\eta$ plane, see [49]. The transverse normal strain, ϵ_{zz}, is not involved in this procedure, and it is directly calculated from the displacements.

Lagrangian functions are chosen as the interpolating functions and are arranged in the following arrays:

$$\begin{aligned} N_{m1} &= \begin{bmatrix} N_{A1} & N_{B1} & N_{C1} & N_{D1} & N_{E1} & N_{F1} \end{bmatrix} \\ N_{m2} &= \begin{bmatrix} N_{A2} & N_{B2} & N_{C2} & N_{D2} & N_{E2} & N_{F2} \end{bmatrix} \\ N_{m3} &= \begin{bmatrix} N_{P} & N_{Q} & N_{R} & N_{S} \end{bmatrix} \end{aligned} \tag{22}$$

Hereinafter, the subscripts $m1$, $m2$, and $m3$ designate quantities computed at the points $(A1, B1, C1, D1, E1, F1)$, $(A2, B2, C2, D2, E2, F2)$, and (P, Q, R, S), respectively. Consequently, the interpolation of strain components is as follows:

$$\begin{aligned} \epsilon_{xx} &= \sum_{m1=1}^{6} N_{m1}\epsilon_{xx_{m1}} = N_{m1}\epsilon_{xx_{m1}} \\ \epsilon_{yy} &= \sum_{m2=1}^{6} N_{m2}\epsilon_{yy_{m2}} = N_{m2}\epsilon_{yy_{m2}} \\ \epsilon_{zz} &= \epsilon_{zz} \\ \epsilon_{yz} &= \sum_{m2=1}^{6} N_{m2}\epsilon_{yz_{m2}} = N_{m2}\epsilon_{yz_{m2}} \\ \epsilon_{xz} &= \sum_{m1=1}^{6} N_{m1}\epsilon_{xz_{m1}} = N_{m1}\epsilon_{xz_{m1}} \\ \epsilon_{xy} &= \sum_{m3=1}^{4} N_{m3}\epsilon_{xy_{m3}} = N_{m3}\epsilon_{xy_{m3}} \end{aligned} \tag{23}$$

where the strains $\epsilon_{xx_{m1}}$, $\epsilon_{yy_{m2}}$, $\epsilon_{xy_{m3}}$, $\epsilon_{xz_{m1}}$, and $\epsilon_{yz_{m2}}$ are determined through Eq. (20), in which the shape functions N_i are evaluated at the tying points.

Thus, the strains components (Eq. (23)) can be extensively written with the CUF (Eq. (13)) and the FEM (Eq. (15)) approximations, adopting the MITC method, as follows:

$$\begin{aligned} \epsilon_{xx} &= \frac{\partial}{\partial x}\left(N_{m1}N_i^{m1}F_{u_x\tau}q_{x_{\tau i}}\right) = N_{m1}N_{i,x}^{m1}F_{u_x\tau}q_{x_{\tau i}} \\ \epsilon_{yy} &= \frac{\partial}{\partial y}\left(N_{m2}N_i^{m2}F_{u_y\tau}q_{y_{\tau i}}\right) = N_{m2}N_{i,y}^{m2}F_{u_y\tau}q_{y_{\tau i}} \\ \epsilon_{zz} &= \frac{\partial}{\partial z}\left(N_i F_{u_z\tau}q_{z_{\tau i}}\right) = N_i F_{u_z\tau,z}q_{z_{\tau i}} \end{aligned}$$

$$
\begin{aligned}
\epsilon_{yz} &= \frac{\partial}{\partial z}\left(N_{m2}N_i^{m2}F_{u_y\tau}q_{y_{\tau i}}\right) + \frac{\partial}{\partial y}\left(N_{m2}N_i^{m2}F_{u_z\tau}q_{z_{\tau i}}\right)\\
&= N_{m2}N_i^{m2}F_{u_y\tau,z}q_{y_{\tau i}} + N_{m2}N_{i,y}^{m2}F_{u_z\tau}q_{z_{\tau i}}\\
\epsilon_{xz} &= \frac{\partial}{\partial z}\left(N_{m1}N_i^{m1}F_{u_x\tau}q_{x_{si}}\right) + \frac{\partial}{\partial x}\left(N_{m1}N_i^{m1}F_{u_z\tau}q_{z_{\tau i}}\right)\\
&= N_{m1}N_i^{m1}F_{u_x\tau,z}q_{x_{\tau i}} + N_{m1}N_{i,x}^{m1}F_{u_z\tau}q_{z_{\tau i}}\\
\epsilon_{xy} &= \frac{\partial}{\partial y}\left(N_{m3}N_i^{m3}F_{u_x\tau}q_{x_{\tau i}}\right) + \frac{\partial}{\partial x}\left(N_{m3}N_i^{m3}F_{u_y\tau}q_{y_{\tau i}}\right)\\
&= N_{m3}N_{i,y}^{m3}F_{u_x\tau}q_{x_{\tau i}} + N_{m3}N_{i,x}^{m3}F_{u_y\tau}q_{y_{\tau i}}
\end{aligned}
\tag{24}
$$

The virtual variations of the strains can be easily written with the proposed notation by using Eqs. (14) and (16). In this case the subscripts $m1$, $m2$, and $m3$ are replaced by $n1$, $n2$, and $n3$. The explicit expressions are given in the following:

$$
\begin{aligned}
\delta\epsilon_{xx} &= \frac{\partial}{\partial x}\left(N_{n1}N_j^{n1}F_{u_xs}\delta q_{x_{sj}}\right) = N_{n1}N_{j,x}^{n1}F_{u_xs}\delta q_{x_{sj}}\\
\delta\epsilon_{yy} &= \frac{\partial}{\partial y}\left(N_{n2}N_j^{n2}F_{u_ys}\delta q_{y_{sj}}\right) = N_{n2}N_{j,y}^{n2}F_{u_ys}\delta q_{y_{sui}}\\
\delta\epsilon_{zz} &= \frac{\partial}{\partial z}\left(N_jF_{u_zs}\delta q_{z_{sj}}\right) = N_jF_{u_zs,z}\delta q_{z_{sj}}\\
\delta\epsilon_{yz} &= \frac{\partial}{\partial z}\left(N_{n2}N_j^{n2}F_{u_ys}\delta q_{y_{sj}}\right) + \frac{\partial}{\partial y}\left(N_{n2}N_j^{n2}F_{u_zs}\delta q_{z_{sj}}\right)\\
&= N_{n2}N_j^{n2}F_{u_ys,z}\delta q_{y_{sj}} + N_{n2}N_{j,y}^{n2}F_{u_zs}\delta q_{z_{sj}}\\
\delta\epsilon_{xz} &= \frac{\partial}{\partial z}\left(N_{n1}N_j^{n1}F_{u_xs}\delta q_{x_{sj}}\right) + \frac{\partial}{\partial x}\left(N_{n1}N_j^{n1}F_{u_zs}\delta q_{z_{sj}}\right)\\
&= N_{n1}N_i^{n1}F_{u_xs,z}\delta q_{x_{sj}} + N_{n1}N_{j,x}^{n1}F_{u_zs}\delta q_{z_{sj}}\\
\delta\epsilon_{xy} &= \frac{\partial}{\partial y}\left(N_{n3}N_j^{n3}F_{u_xs}\delta q_{x_{sj}}\right) + \frac{\partial}{\partial x}\left(N_{n3}N_j^{n3}F_{u_ys}\delta q_{y_{sj}}\right)\\
&= N_{n3}N_{j,y}^{n3}F_{u_xs}\delta q_{x_{sj}} + N_{n3}N_{j,x}^{n3}F_{u_ys}\delta q_{y_{sj}}
\end{aligned}
\tag{25}
$$

4.2. Governing equations

The principle of virtual displacement (see the classical work of Washizu [20] for more details) is used to derive the governing equations, which reads:

$$
\delta L_{int} = \delta L_{ext} \tag{26}
$$

First, the virtual internal work is considered and its expression is given by:

$$
\delta L_{int} = \int_V \delta\boldsymbol{\epsilon}^T\boldsymbol{\sigma}\mathrm{d}V = \int_V \left(\delta\epsilon_{xx}\sigma_{xx} + \delta\epsilon_{yy}\sigma_{yy} + \delta\epsilon_{zz}\sigma_{zz} + \delta\epsilon_{yz}\sigma_{yz} + \delta\epsilon_{xz}\sigma_{xz} + \delta\epsilon_{xy}\sigma_{xy}\right)\mathrm{d}V \tag{27}
$$

where $\mathrm{d}V = \mathrm{d}x\mathrm{d}y\mathrm{d}z$. Using the MITC method (Eqs. (24) and (25)), the CUF and the FEM approximations (Eqs. (15) and (16)), and the constitutive equations (Eq. (21)), the expression for the internal work reads:

$$
\begin{aligned}
&\delta L_{int} =\\
&+\delta q_{x_{sj}}C_{11}N_{j,x}^{n1}N_{i,x}^{m1}\int_\Omega N_{n1}N_{m1}\mathrm{d}x\mathrm{d}y\int_A F_{u_xs}F_{u_x\tau}\mathrm{d}z\,q_{x_{\tau i}} + \delta q_{x_{sj}}C_{12}N_{j,y}^{n2}N_{i,x}^{m1}\int_\Omega N_{n2}N_{m1}\mathrm{d}x\mathrm{d}y\int_A F_{u_xs}F_{u_y\tau}\mathrm{d}z\,q_{y_{\tau i}}\\
&+\delta q_{x_{sj}}C_{13}N_{i,x}^{m1}\int_\Omega N_jN_{m1}\mathrm{d}x\mathrm{d}y\int_A F_{u_xs,z}F_{u_z\tau}\mathrm{d}z\,q_{z_{\tau i}} + \delta q_{y_{sj}}C_{12}N_{j,x}^{n1}N_{i,y}^{m2}\int_\Omega N_{n1}N_{m2}\mathrm{d}x\mathrm{d}y\int_A F_{u_ys}F_{u_x\tau}\mathrm{d}z\,q_{x_{\tau i}}\\
&+\delta q_{y_{sj}}C_{22}N_{j,y}^{n2}N_{i,y}^{m2}\int_\Omega N_{n2}N_{m2}\mathrm{d}x\mathrm{d}y\int_A F_{u_ys}F_{u_y\tau}\mathrm{d}z\,q_{y_{\tau i}} + \delta q_{y_{sj}}C_{23}N_{i,y}^{m2}\int_\Omega N_jN_{m2}\mathrm{d}x\mathrm{d}y\int_A F_{u_ys,z}F_{u_z\tau}\mathrm{d}z\,q_{z_{\tau i}}\\
&+\delta q_{x_{sj}}C_{66}N_{j,y}^{n3}N_{i,y}^{m3}\int_\Omega N_{n3}N_{m3}\mathrm{d}x\mathrm{d}y\int_A F_{u_xs}F_{u_x\tau}\mathrm{d}z\,q_{x_{\tau i}} + \delta q_{y_{sj}}C_{66}N_{j,y}^{n3}N_{i,x}^{m3}\int_\Omega N_{n3}N_{m3}\mathrm{d}x\mathrm{d}y\int_A F_{u_ys}F_{u_x\tau}\mathrm{d}z\,q_{x_{\tau i}}\\
&+\delta q_{x_{sj}}C_{66}N_{j,x}^{n3}N_{i,y}^{m3}\int_\Omega N_{n3}N_{m3}\mathrm{d}x\mathrm{d}y\int_A F_{u_xs}F_{u_y\tau}\mathrm{d}z\,q_{y_{\tau i}} + \delta q_{y_{sj}}C_{66}N_{j,x}^{n3}N_{i,x}^{m3}\int_\Omega N_{n3}N_{m3}\mathrm{d}x\mathrm{d}y\int_A F_{u_ys}F_{u_y\tau}\mathrm{d}z\,q_{y_{\tau i}}\\
&+\delta q_{z_{sj}}C_{44}N_{j,y}^{n2}N_{i,y}^{m2}\int_\Omega N_{n2}N_{m2}\mathrm{d}x\mathrm{d}y\int_A F_{u_zs}F_{u_z\tau}\mathrm{d}z\,q_{z_{\tau i}} + \delta q_{y_{sj}}C_{44}N_{j,y}^{n2}N_i^{m2}\int_\Omega N_{n2}N_{m2}\mathrm{d}x\mathrm{d}y\int_A F_{u_ys}F_{u_z\tau,z}\mathrm{d}z\,q_{z_{\tau i}}\\
&+\delta q_{z_{sj}}C_{44}N_j^{n2}N_{i,y}^{m2}\int_\Omega N_{n2}N_{m2}\mathrm{d}x\mathrm{d}y\int_A F_{u_zs,z}F_{u_y\tau}\mathrm{d}z\,q_{y_{\tau i}} + \delta q_{y_{sj}}C_{44}N_j^{n2}N_i^{m2}\int_\Omega N_{n2}N_{m2}\mathrm{d}x\mathrm{d}y\int_A F_{u_ys,z}F_{u_y\tau,z}\mathrm{d}z\,q_{y_{\tau i}}\\
&+\delta q_{z_{sj}} + C_{55}N_{j,x}^{n1}N_{i,x}^{m1}\int_\Omega N_{n1}N_{m1}\mathrm{d}x\mathrm{d}y\int_A F_{u_zs}F_{u_z\tau}\mathrm{d}z\,q_{z_{\tau i}} + \delta q_{x_{sj}}C_{55}N_{j,x}^{n1}N_i^{m1}\int_\Omega N_{n1}N_{m1}\mathrm{d}x\mathrm{d}y\int_A F_{u_xs,x}F_{u_z\tau,z}\mathrm{d}z\,q_{z_{\tau i}}\\
&+\delta q_{z_{sj}}C_{55}N_j^{n1}N_{i,x}^{m1}\int_\Omega N_{n1}N_{m1}\mathrm{d}x\mathrm{d}y\int_A F_{u_zs,z}F_{u_x\tau}\mathrm{d}z\,q_{x_{\tau i}} + \delta q_{x_{sj}}C_{55}N_j^{n1}N_i^{m1}\int_\Omega N_{n1}N_{m1}\mathrm{d}x\mathrm{d}y\int_A F_{u_xs,z}F_{u_x\tau,z}\mathrm{d}z\,q_{x_{\tau i}}
\end{aligned}
$$

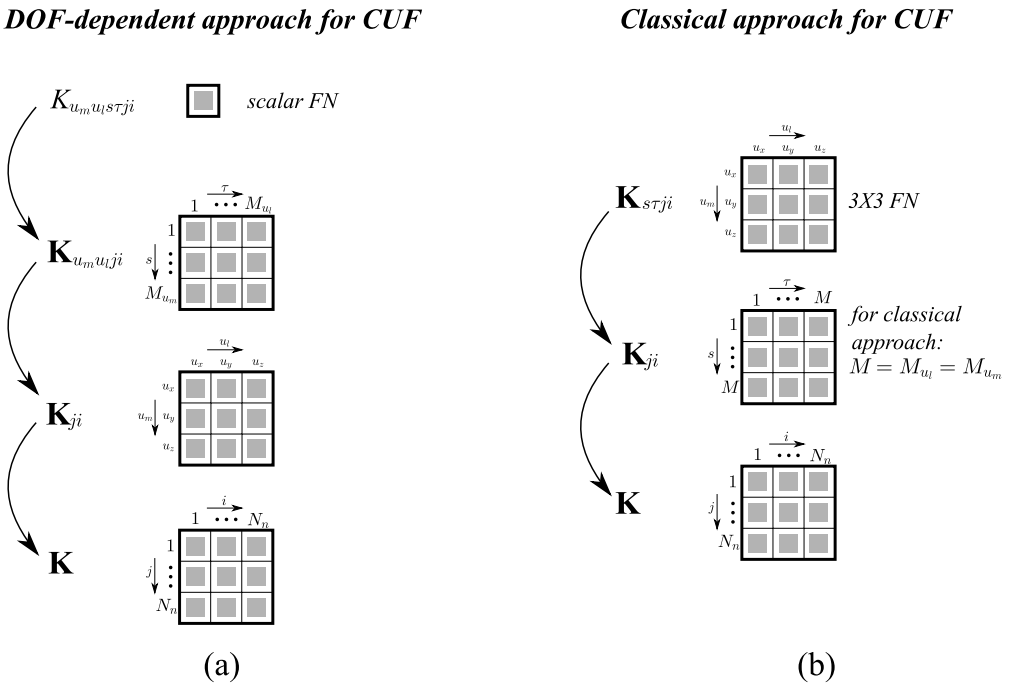

Fig. 10. Assembly of the stiffness matrix for the novel approach (a) and classical CUF (b), starting from the fundamental nuclei.

$$+\delta q_{z_{sj}} C_{13} N^{n1}_{j,x} \int_\Omega N_{n1} N_i \mathrm{d}x\mathrm{d}y \int_A F_{u_z s} F_{u_x \tau,z} \mathrm{d}z \; q_{x_{\tau i}} + \delta q_{z_{sj}} C_{23} N^{n2}_{j,y} \int_\Omega N_{n2} N_i \mathrm{d}x\mathrm{d}y \int_A F_{u_z s} F_{u_y \tau,z} \mathrm{d}z \; q_{y_{\tau i}}$$
$$+\delta q_{z_{sj}} C_{33} \int_\Omega N_j N_i \mathrm{d}x\mathrm{d}y \int_A F_{u_z s,z} F_{u_z \tau,z} \mathrm{d}z \; q_{z_{\tau i}} \tag{28}$$

Second, considering the virtual external work from point loads:

$$\delta L_{ext} = \delta \mathbf{u}^T \mathbf{P} = \left(\delta u_x P_{u_x} + \delta u_y P_{u_y} + \delta u_z P_{u_z} \right) \tag{29}$$

Inserting the CUF and FEM (Eq. (16)) approximations the external work is given by:

$$\begin{aligned} \delta L_{ext} =& \delta q_{x_{sj}} N_j F_{u_x s} P_{u_x} + \delta q_{y_{sj}} N_j F_{u_y s} P_{u_y} + \delta q_{z_{sj}} N_j F_{u_z s} P_{u_z} \\ =& \delta q_{x_{sj}} P_{u_x sj} + \delta q_{y_{sj}} P_{u_y sj} + \delta q_{z_{sj}} P_{u_z sj} \end{aligned} \tag{30}$$

where $P_{u_x sj} = N_j F_{u_x s} P_{u_x}$, $P_{u_y sj} = N_j F_{u_y s} P_{u_y}$, and $P_{u_z sj} = N_j F_{u_z s} P_{u_z}$.

Thus, three distinct governing equations can be derived:

$$\begin{aligned} \delta q_{x_{sj}} &: K_{u_x u_x s\tau ji} q_{x_{\tau i}} + K_{u_x u_y s\tau ji} q_{y_{\tau i}} + K_{u_x u_z s\tau ji} q_{z_{\tau i}} = P_{u_x sj} \\ \delta q_{y_{sj}} &: K_{u_y u_x s\tau ji} q_{x_{\tau i}} + K_{u_y u_y s\tau ji} q_{y_{\tau i}} + K_{u_y u_z s\tau ji} q_{z_{\tau i}} = P_{u_y sj} \\ \delta q_{z_{sj}} &: K_{u_z u_x s\tau ji} q_{x_{\tau i}} + K_{u_z u_y s\tau ji} q_{y_{\tau i}} + K_{u_z u_z s\tau ji} q_{z_{\tau i}} = P_{u_z sj} \end{aligned}$$

For the sake of completeness, the nine fundamental nuclei of the stiffness matrix are written explicitly in Appendix.

4.3. Stiffness matrix

In this work, the scalar $K_{u_m u_l s\tau ji}$ is the Fundamental Nucleus (FN) of the stiffness matrix. Consequently, the theory consists of nine independent scalar algebraic equations. In contrast, previous CUF-based papers [2] used a 3×3 submatrix as the kernel. This modification allows for the individual treatment of each displacement variable, enhancing the flexibility and adaptability of the model.

Fig. 10 illustrates the differences between the two methods during the assembly of the stiffness matrix. In the current approach, see Fig. 10 a, the invariant kernel is expanded with respect to s and τ. Subsequently, the resulting submatrix undergoes expansion with respect to u_m and u_l, followed by another expansion with respect to j and i to form the final structural matrix. In contrast, the 'classical procedure', depicted in Fig. 10 b, incorporates the loops on the displacement variables within the 3×3 FN, where $K_{u_m u_l}$ is a component of the matrix $\mathbf{K}_{s\tau ji}$. In this method, the nucleus is initially expanded with respect to s and τ, followed by an expansion of the resulting submatrix with respect to j and i to form the final structural matrix.

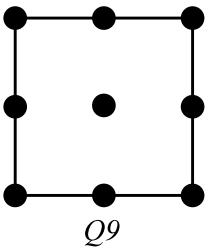

$$\text{TE4:}\quad u_x = u_{x_1} + zu_{x_2} + z^2u_{x_3} + z^3u_{x_4} + z^4u_{x_5} \qquad M_{u_x} = 5$$

$$\text{TE4:}\quad u_y = u_{y_1} + zu_{y_2} + z^2u_{y_3} + z^3u_{y_4} + z^4u_{y_5} \qquad M_{u_y} = 5$$

$$\text{TE1:}\quad u_z = u_{z_1} + zu_{z_2} \qquad M_{u_z} = 2$$

Fig. 11. Example of a plate element. u_x and u_y are studied by using a fourth-order model (TE4), whereas a linear model (TE1) approximates the displacement variable u_z.

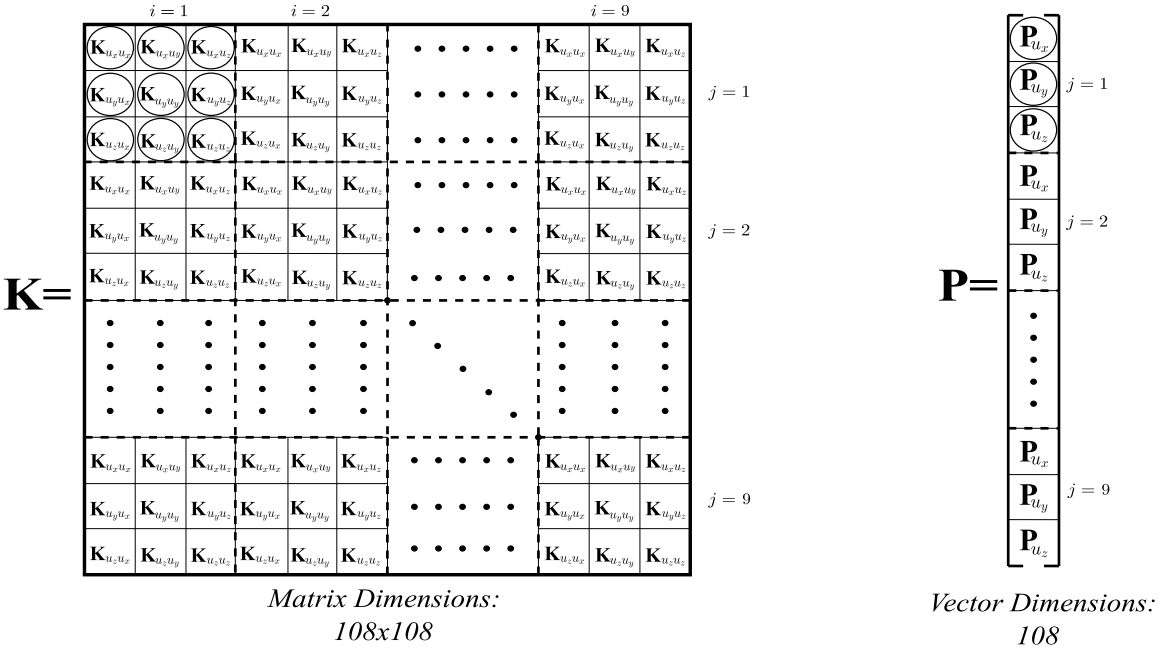

Fig. 12. Assembly of the general stiffness matrix and the general load vector. See details of $\mathbf{K}_{11}$ and $\mathbf{P}_1$ in Fig. 13.

5. Assembly

This section presents an example to show the assembly of the matrices in the present context of the Unified formulation. To understand the process, an example is taken into account. Fig. 11 illustrates a nine-node element (Q9). The structural theories is also shown in the figure, where u_x and u_y are studied by using a fourth-order model, while the model TE1 approximates the variable u_z. In this way, $M_{u_x} = M_{u_y} = 5$ and $M_{u_z} = 2$. Thence, 12 Degrees of Freedom (DOF) are used for each FE node. The total DOF are 108. Fig. 12 shows the stiffness matrix, with dimensions 108×108, and the load vector, with dimensions 108, of the entire structure. Each submatrix $\mathbf{K}_{ji}$ is subdivided into nine submatrices, while each subvector $\mathbf{P}_j$ is composed by three smaller subvectors. As example, Fig. 13 clearly illustrates the nine components of $\mathbf{K}_{11}$ and the three components $\mathbf{P}_1$. The dimension and the shape of the matrices $\mathbf{K}_{u_m u_l}11$ depend on the number of terms in the models adopted for each displacement variable. $\mathbf{K}_{u_x u_x}11$, $\mathbf{K}_{u_y u_x}11$, $\mathbf{K}_{u_x u_y}11$ and $\mathbf{K}_{u_y u_y}11$ are square 5×5 matrices, since M_{u_x} and M_{u_y} are equal to 5. $\mathbf{K}_{u_z u_z}11$ is squared with dimensions 2×2, because $M_{u_z} = 2$. The use of different M for the variables leads to rectangular $\mathbf{K}_{u_m u_l}11$ with different dimensions, as in the case of matrices $\mathbf{K}_{u_x u_z}11$, $\mathbf{K}_{u_y u_z}11$, $\mathbf{K}_{u_z u_x}11$ and $\mathbf{K}_{u_z u_y}11$. Each 1×1 fundamental nucleus corresponds to the real components of the matrices. A similar procedure can be followed for the load vector.

6. Numerical results

This section explores four benchmarks that focus on the study of displacements and stresses. The first benchmark involves a simply-supported square plate, followed by a plate with unitary width subjected to cylindrical bending. End-effects in a clamped plate are considered in the third case. Lastly, a plate subjected to a localized pressure is analysed. In this manner, various loadings and

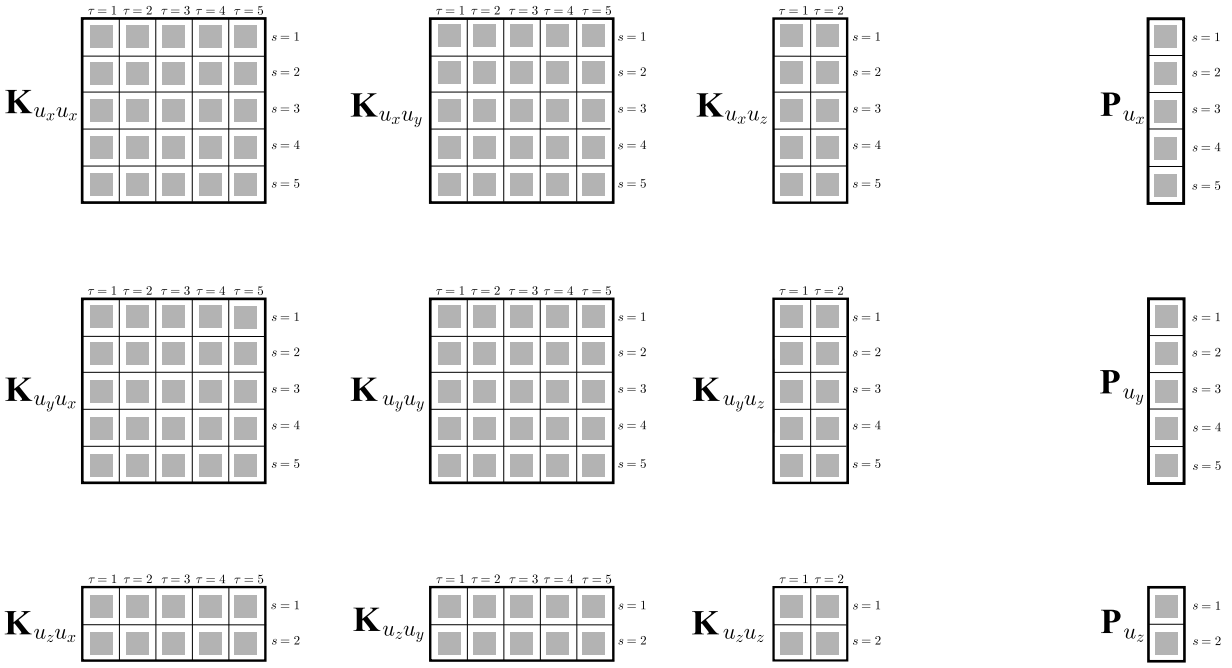

Fig. 13. Assembly of the stiffness matrix (submatrix $\mathbf{K}_{11}$) and the load vector (subvector $\mathbf{P}_1$).

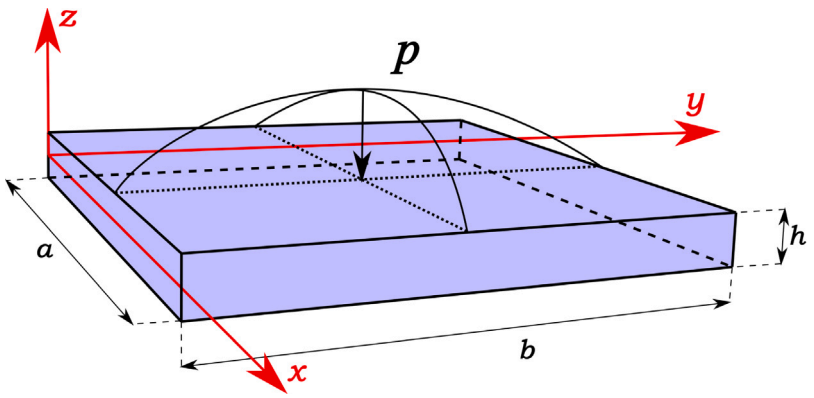

Fig. 14. Geometrical properties of Benchmark 1. Simply-supported metallic square plate under distributed bi-sinusoidal pressure.

boundary conditions are considered. Additionally, a range of length-to-thickness ratios, from very thick to very thin, is considered. To address the shear locking problem, the MITC integration scheme is employed.

Since the present method is able to build many theories, a consistent acronym system is proposed. When the *uniform* and the *reduced* models are referred to, the following notation is adopted: TEn_{u_x}-TEn_{u_y}-TEn_{u_z}, where n_{u_l} indicates the polynomial for each displacement component. For example, TE2-TE5-TE3 stands for:

- TE2: second-order Taylor expansion for u_x;
- TE5: fifth-order Taylor expansion for u_y;
- TE3: third-order Taylor expansion for u_z.

Furthermore, TE0 indicates that only the constant term is employed in the expansion.

When the *reduced* models are utilized, they are defined during the expositions of the benchmarks. In fact, these models are explicitly written for the sake of clarity.

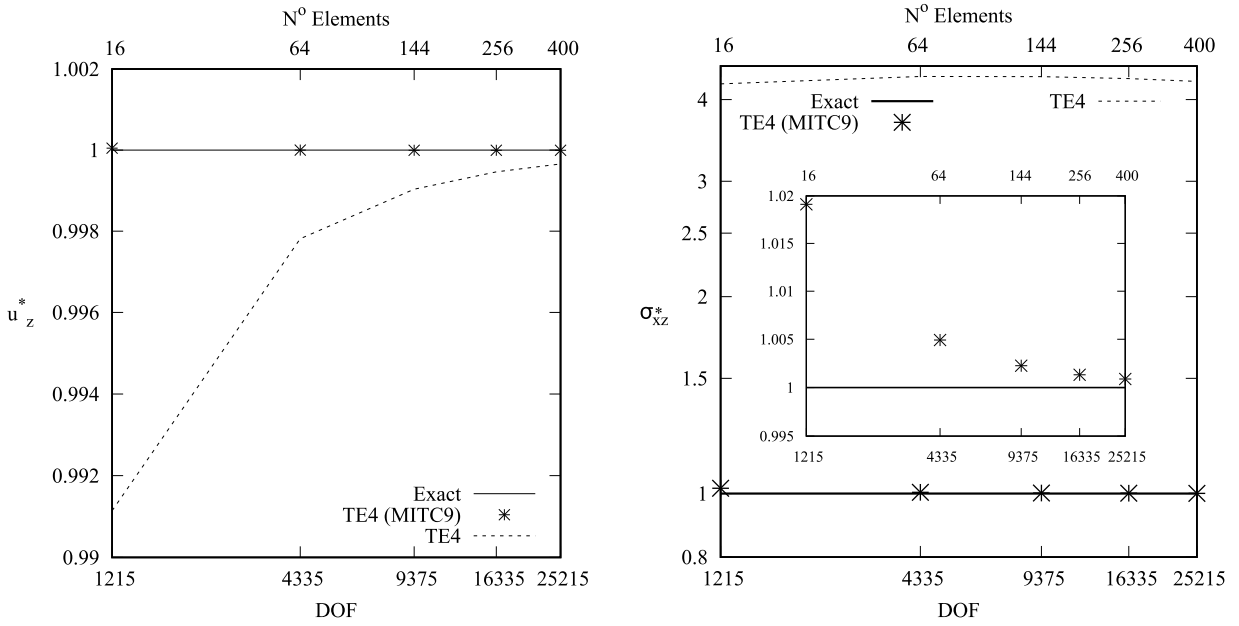

(a) Transverse displacement in $[a/2, b/2, 0]$. (b) Shear stress in $[a/2, b, 0]$.

Fig. 15. Simply-supported metallic square plate under distributed bi-sinusoidal pressure. Case $a/h = 1000$. Convergence analysis.

6.1. Bending of a square plate

The first example involves a square metallic plate with equal sides, denoted by $a = b$. Illustrated in Fig. 14, various length-to-thickness ratios, specifically $a/h = 2, 4, 10, 100, 1000$, are examined. The material is isotropic with the following properties: $E = 73$ [GPa] and $\nu = 0.34$. The plate, simply supported on all four edges, is subjected to a bi-sinusoidal pressure $p = p_z \sin\left(\frac{\pi x}{a}\right) \sin\left(\frac{\pi y}{b}\right)$, with a mechanical load amplitude of $p_z = 1$ [Pa] at the top position. The study evaluates non-dimensional transverse displacements, $\overline{u}_z$, along with in-plane stress, $\overline{\sigma}_{xx}$, and shear stress, $\overline{\sigma}_{xz}$. $\overline{u}_z$ and $\overline{\sigma}_{xx}$ are calculated in $[a/2, b/2, z]$, while $\overline{\sigma}_{xz}$ are evaluated in $[a/2, b, z]$. Displacements and stresses are given in the following non-dimensional form:

$$\overline{u}_z = \frac{100\ E\ u_z}{p_z \left(\frac{a}{h}\right)^4 h} \qquad \overline{\sigma}_{xx} = \frac{\sigma_{xx}}{p_z \left(\frac{a}{h}\right)^2} \qquad \overline{\sigma}_{xz} = \frac{\sigma_{xz}}{p_z \left(\frac{a}{h}\right)} \tag{31}$$

Results are compared with a closed-form Navier-type solution termed 'Exact,' built using the strong-form governing equations in the CUF framework. The analytical Navier solution is possible given the absence of mechanical couplings in simply supported structures. A fourth-order Taylor theory is employed throughout the thickness, and additional details can be found in [19].

Exploiting geometric and loading symmetries, a quarter of the plate is studied, allowing for a reduction in computational costs.

A convergence mesh analysis is conducted for the $a/h = 1000$ case, employing TE4-TE4-TE4 as the structural theory. For the sake of brevity, it is termed as TE4. Fig. 15 presents the results in terms of both Degrees of Freedom (DOF) and the number of elements (N° Elements). The 'Exact' model serves as the reference result, with transverse displacements and shear stresses taken as control parameters. The results are normalized as follows:

$$u_z^* = \frac{\overline{u}_z}{\overline{u}_z(\text{Exact})} \qquad \sigma_{xz}^* = \frac{\overline{\sigma}_{xz}}{\overline{\sigma}_{xz}(\text{Exact})} \tag{32}$$

Comparisons are made between two integration techniques, namely the Full scheme (without any shear locking correction technique) and MITC. 20×20 MITC (25215 DOF for the specific case of the uniform TE4 model) is chosen as the FE mesh discretization which will be consistently employed for each length-to-thickness ratio to ensure fair comparison.

Fig. 16 illustrates the relationship between the length-to-thickness ratio, a/h, and the transverse displacement, $\overline{u}_z$, using uniform and different theories. Since the plate is square, the material is isotropic, and the boundary conditions are symmetric, the in-plane displacement variables (u_x and u_y) always have identical expansions. These analyses provide an opportunity to highlight the role of Poisson Locking. This phenomenon occurs when TE0 or TE1 expansions are used for the u_z displacement variable, even if higher-order terms are used for u_x and u_y. This crucial problem can be addressed using two different strategies:

1. The elastic coefficients are modified. In this analyses, two superscripts are used: 'no Corr' indicates a model where the Poisson Locking is not corrected, while 'Corr' corresponds to models where the correction is applied. See the book [51] for more information.

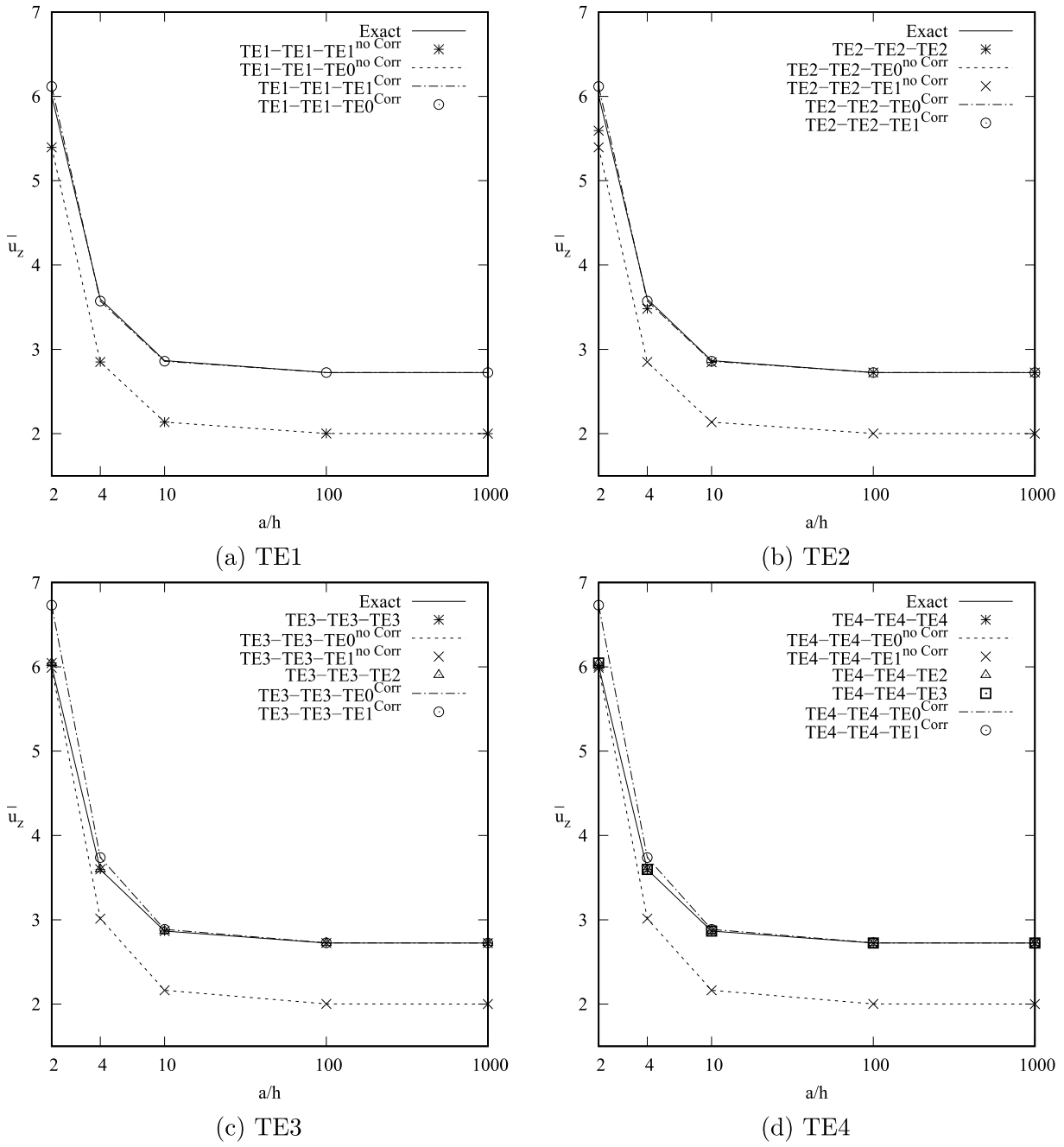

Fig. 16. Simply-supported metallic square plate under distributed bi-sinusoidal pressure. Relationship between length-to-thickness ratio, a/h, and the transverse displacement, $\bar{u}_z$ (evaluated in $[a/2, b/2, 0]$).

2. Adding a parabolic term to the u_z variable (TE2) is sufficient, albeit with an increase in computational costs;

The figures highlight that both corrections improve the results. It is interesting to note that the Poisson Locking issue becomes more significant as the plate becomes thinner. Hereafter, only the 'corrected' models are used when the linear (or constant) expansion is considered for the transverse variable. The superscripts 'Corr' will not be written for the sake of conciseness.

Finally, attention is focused on two length-to-thickness ratios, $a/h = 4$ and $a/h = 100$. Tables 4 and 5 illustrate the results for the thick and thin plate, respectively. The first three columns show the models used, and the fourth column displays the number of terms for each variable. Subsequently, the results for displacements and stresses are presented. Transverse displacements, $\bar{u}_z$, are evaluated at $[a/2, b/2, 0]$. In-plane stresses, $\bar{\sigma}_{xx}$, and shear stresses, $\bar{\sigma}_{xz}$, are calculated at $[a/2, b/2, h/2]$ and $[a/2, b, 0]$, respectively.

Table 4
Simply-supported metallic square plate under distributed bi-sinusoidal pressure. Case $a/h = 4$.

Model u_x	Model u_y	Model u_z	$M_{u_x}/M_{u_y}/M_{u_z}$	$\bar{u}_z$ [a]	$\bar{\sigma}_{xx}$ [b]	$\bar{\sigma}_{xz}$ [c]	DOF
Exact							
TE4	TE4	TE4	—[d]	3.5958	0.2252	0.2369	—[e]
Uniform Models							
TE1	TE1	TE1	2/2/2	3.5723	0.2117	0.1592	10086
TE2	TE2	TE2	3/3/3	3.4815	0.2176	0.1700	15129
TE3	TE3	TE3	4/4/4	3.5976	0.2339	0.2364	20172
TE4	TE4	TE4	5/5/5	3.5959	0.2253	0.2370	25125
Different Models							
TE1	TE1	TE0	2/2/1	3.5723	0.2037	0.1592	8405
TE2	TE2	TE0	3/3/1	3.5723	0.2037	0.1592	11767
TE2	TE2	TE1	3/3/2	3.5723	0.2144	0.1592	13448
TE3	TE3	TE0	4/4/1	3.7376	0.2161	0.2368	15129
TE3	TE3	TE1	4/4/2	3.7376	0.2267	0.2368	16810
TE3	TE3	TE2	4/4/3	3.5976	0.2349	0.2364	18491
TE4	TE4	TE0	5/5/1	3.7376	0.2161	0.2368	18491
TE4	TE4	TE1	5/5/2	3.7376	0.2267	0.2368	20172
TE4	TE4	TE2	5/5/3	3.5976	0.2349	0.2364	21853
TE4	TE4	TE3	5/5/4	3.5976	0.2339	0.2364	23534
TE2	TE2	TE4	3/3/5	3.4813	0.2162	0.1700	18491
Reduced Models							
Model 1			3/3/4	3.5959	0.2230	0.2370	16810
Model 2			4/4/4	3.5959	0.2262	0.2370	20172

[a] Computed at $[a/2, b/2, 0]$.
[b] Computed at $[a/2, b/2, h/2]$.
[c] Computed at $[a/2, b, 0]$.
[d] M's are not reported for the exact theory.
[e] Closed-form solution.

Table 5
Simply-supported metallic square plate under distributed bi-sinusoidal pressure. Case $a/h = 100$.

Model u_x	Model u_y	Model u_z	$M_{u_x}/M_{u_y}/M_{u_z}$	$\bar{u}_z$ [a]	$\bar{\sigma}_{xx}$ [b]	$\bar{\sigma}_{xz}$ [c]	DOF
Exact							
LM4	LM4	LM4	—[d]	2.7252	0.2038	0.2389	—[e]
Uniform Models							
TE1	TE1	TE1	2/2/2	2.7251	0.2038	0.1593	10086
TE2	TE2	TE2	3/3/3	2.7250	0.2037	0.1728	15129
TE3	TE3	TE3	4/4/4	2.7252	0.2038	0.2389	20172
TE4	TE4	TE4	5/5/5	2.7252	0.2038	0.2389	25125
Different Models							
TE1	TE1	TE0	2/2/1	2.7251	0.2037	0.1593	8405
TE2	TE2	TE0	3/3/1	2.7251	0.2037	0.1593	11767
TE2	TE2	TE1	3/3/2	2.7251	0.2037	0.1593	13448
TE3	TE3	TE0	4/4/1	2.7254	0.2038	0.2389	15129
TE3	TE3	TE1	4/4/2	2.7254	0.2038	0.2389	16810
TE3	TE3	TE2	4/4/3	2.7252	0.2038	0.2389	18491
TE4	TE4	TE0	5/5/1	2.7254	0.2038	0.2389	18491
TE4	TE4	TE1	5/5/2	2.7254	0.2038	0.2389	20172
TE4	TE4	TE2	5/5/3	2.7252	0.2038	0.2389	21853
TE4	TE4	TE3	5/5/4	2.7252	0.2038	0.2389	23534
TE2	TE2	TE4	3/3/5	2.7252	0.2037	0.1728	18491

[a] Computed at $[a/2, b/2, 0]$.
[b] Computed at $[a/2, b/2, h/2]$.
[c] Computed at $[a/2, b, 0]$.
[d] M's are not reported for the exact theory.
[e] Closed-form solution.

Then, the DOFs are presented for comparison purposes. The 'Exact' reference solutions, and *different*, *uniform*, and *reduced* models are compared. The number of terms and DOFs are not indicated for the closed-form solution. For different models, as shown in Fig. 16, the in-plane displacement variables are considered equal. Specifically, TE2-TE2-TE4 is proposed to demonstrate the importance of higher-order terms for the in-plane displacements in achieving excellent results. In addition to the different and complete models, two *reduced* theories are presented, which can achieve results similar to the reference solution with fewer expansion terms:

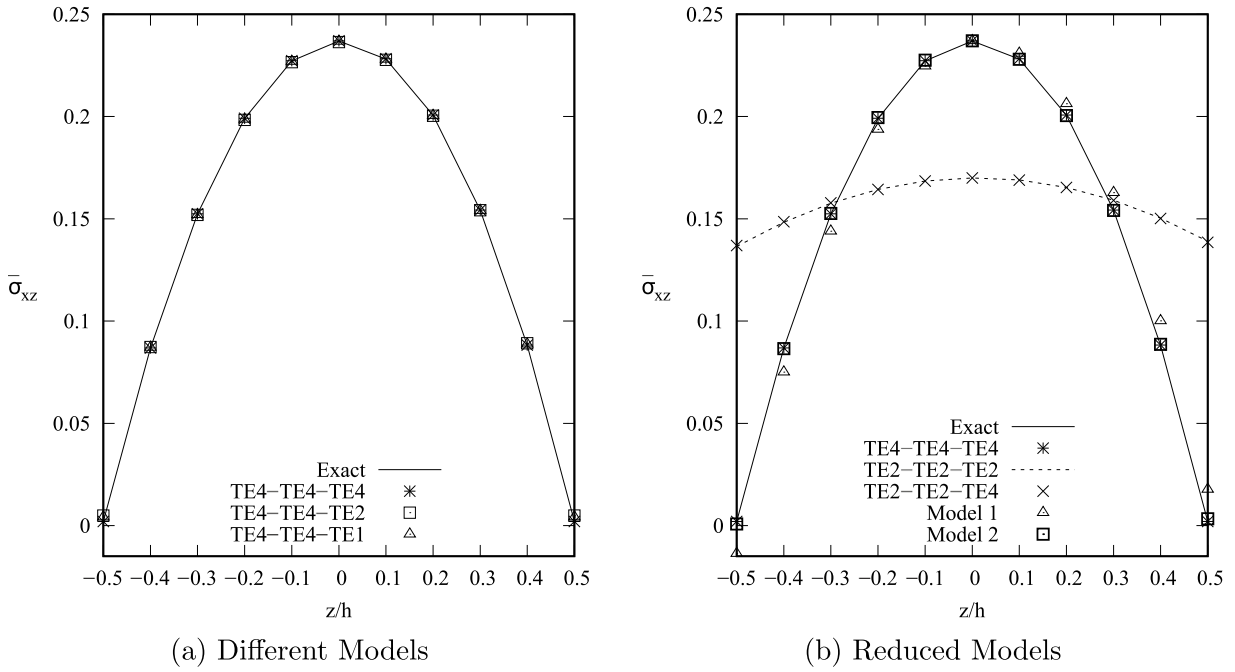

Fig. 17. Simply-supported metallic square plate under distributed bi-sinusoidal pressure. Case $a/h = 4$. Shear stresses, $\overline{\sigma}_{xz}$, evaluated in $[a/2, b, z]$.

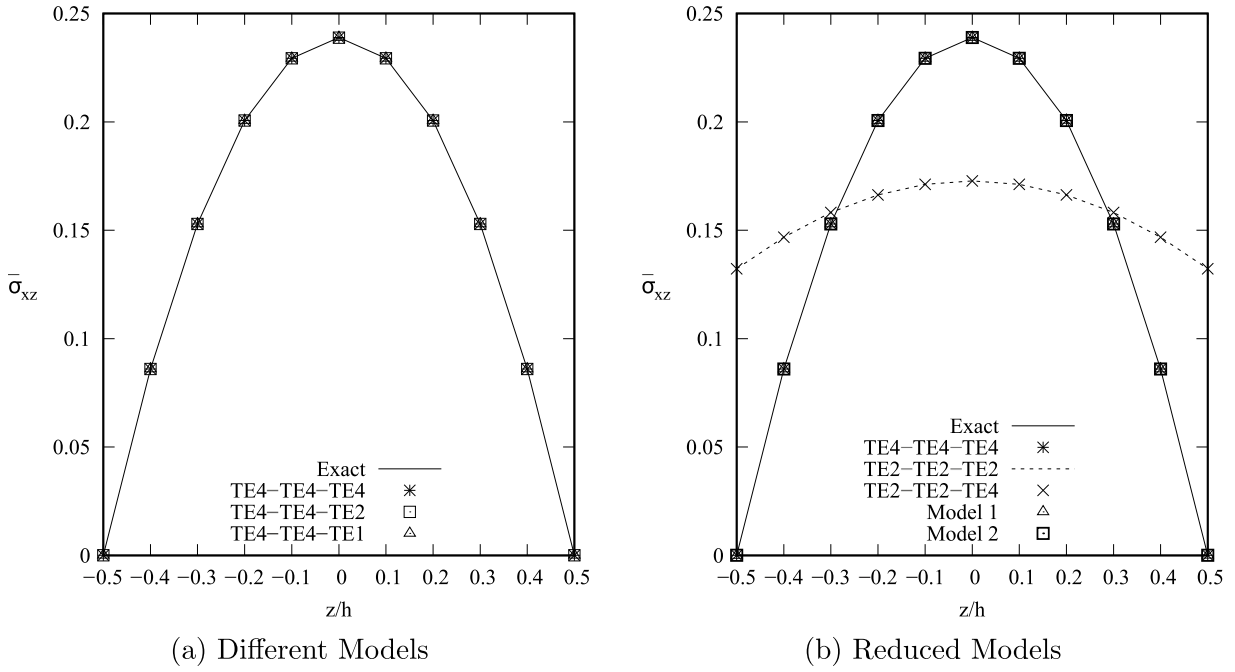

Fig. 18. Simply-supported metallic square plate under distributed bi-sinusoidal pressure. Case $a/h = 100$. Shear stresses, $\overline{\sigma}_{xz}$, evaluated in $[a/2, b, z]$.

$$\text{Model 1:} \quad \begin{aligned} u_x &= u_{x_1} + z u_{x_2} + z^3 u_{x_3} \\ u_y &= u_{y_1} + z u_{y_2} + z^3 u_{y_3} \\ u_z &= u_{z_1} + z u_{z_2} + z^2 u_{z_3} + z^4 u_{z_4} \end{aligned} \tag{33}$$

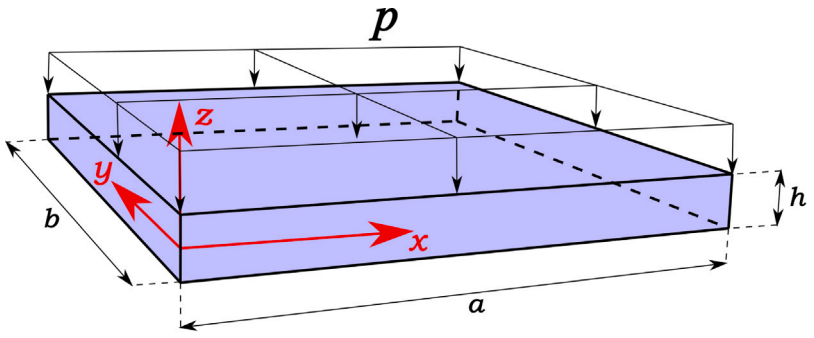

Fig. 19. Geometrical properties of Benchmark 2. Simply-supported metallic plate under distributed constant pressure.

$$\text{Model 2:} \quad \begin{aligned} u_x &= u_{x_1} + zu_{x_2} + z^2u_{x_3} + z^3u_{x_4} \\ u_y &= u_{y_1} + zu_{y_2} + z^2u_{y_3} + z^3u_{y_4} \\ u_z &= u_{z_1} + zu_{z_2} + z^2u_{z_3} + z^4u_{z_4} \end{aligned} \tag{34}$$

Figs. 17 and 18 illustrate the trends of the shear stresses, $\overline{\sigma}_{xz}$, for the thick and the thin plate, respectively. For the sake of brevity, only some interesting models are shown. When TE4 is adopted for the u_x and u_y variables, the results are in agreement with the reference solutions. Optimal outcomes can be obtained if third-order expansions are used for the in-plane displacements, as seen for Models 1 and 2.

Several important observations can be made based on the results:

- The analysis highlights the necessity for refined models to achieve results that closely match the reference solution;
- Thanks to the *reduced* models, it is possible to obtain good results, but with less DOF;
- The terms of the in-plane displacement variables are the most significant in the solution. On the contrary, the problem exhibits less sensitivity to the model for u_z;
- The behaviour of the outputs $\overline{u}_z$ and $\overline{\sigma}_{xx}$ is strongly influenced by the ratio a/h. In fact, several terms are needed to obtain excellent results if the plate is thick, while few DOF are sufficient for the thin plate. Conversely, the shear stresses, $\overline{\sigma}_{xz}$, exhibit almost the same trends for the two length-to-thickness ratios.

6.2. Cylindrical bending of a plate

A metallic plate is analysed as the second example. The benchmark is presented in this work for the first time. The geometric and loading conditions are described in Fig. 19. Several length-to-thickness ratios are studied, $a/h = 2, 4, 10, 100, 1000$. The width b is unitary. The material is the same of the previous example. The plate is simply-supported on the edges along the y-direction and it is loaded with a constant pressure, with $p_z = 1$ [Pa]. The study evaluates non-dimensional transverse displacements, $\overline{u}_z$, along with in-plane stress, $\overline{\sigma}_{xx}$, and shear stress, $\overline{\sigma}_{xz}$. In particular, $\overline{u}_z$ and $\overline{\sigma}_{xz}$ are calculated in $[a/2, b/2, z]$, while $\overline{\sigma}_{xz}$ is evaluated in $[a, b/2, z]$. For comparison purposes, displacements and stresses are given in non-dimensional form as follows:

$$\overline{u}_z = \frac{10\ E\ u_z}{p_z \left(\frac{a}{h}\right)^4 h} \qquad \overline{\sigma}_{xx} = \frac{\sigma_{xx}}{p_z \left(\frac{a}{h}\right)^2} \qquad \overline{\sigma}_{xz} = \frac{\sigma_{xz}}{p_z \left(\frac{a}{h}\right)} \tag{35}$$

When the maximum term for the u_z displacement variable is linear, the Poisson Locking correction is activated, as in the previous benchmark.

A convergence analysis is performed for the case $a/h = 1000$ by using TE4-TE4-TE4 as structural theory to set the reference solution and the number of FE. One element is chosen along the y axis, while elements are added along the x direction. Fig. 20 shows the outcomes. Transverse displacements and in-plane stresses, are taken as the parameters. The results are normalized as follows:

$$u_z^* = \frac{\overline{u}_z}{\overline{u}_z(60 \times 1 \text{ MITC})} \qquad \sigma_{xx}^* = \frac{\overline{\sigma}_{xx}}{\overline{\sigma}_{xx}(60 \times 1 \text{ MITC})} \tag{36}$$

Both the Full scheme and MITC integration techniques are compared. 30×1 MITC (or 2745 DOF) is chosen as the FE mesh discretization. In the following analyses, this mesh configuration will be used for all the length-to-thickness ratios.

After choosing the FE discretization, two length-to-thickness ratios, $a/h = 4$ and $a/h = 100$, are considered. Tables 6 and 7 present the results for the thick and thin plate, respectively. As in the previous benchmark, the first three columns show the models used, and the fourth column displays the number of terms. Then, the results for the displacements and stresses are presented. Transverse displacements, $\overline{u}_z$, are evaluated at $[a/2, b/2, 0]$. In-plane stresses, $\overline{\sigma}_{xx}$, and shear stresses, $\overline{\sigma}_{xz}$, are calculated at $[a/2, b/2, h/2]$ and $[a, b/2, 0]$, respectively. Finally, DOFs are provided for comparison purposes. The *uniform* model TE4-TE4-TE4 is taken as the reference solution.

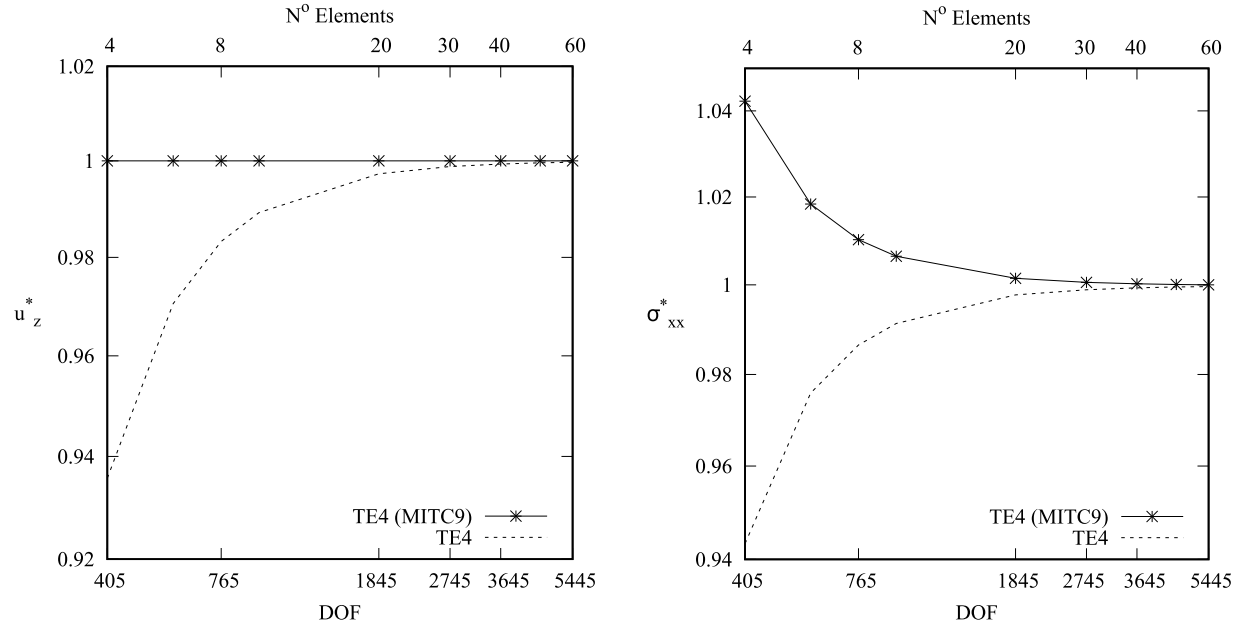

(a) Transverse displacement in $[a/2, b/2, 0]$. (b) In-plane stress in $[a/2, b/2, h/2]$.

Fig. 20. Simply-supported metallic plate under distributed constant pressure. Case $a/h = 1000$. Convergence analysis.

Table 6
Simply-supported metallic plate under distributed constant pressure. Case $a/h = 4$.

Model u_x	Model u_y	Model u_z	$M_{u_x}/M_{u_y}/M_{u_z}$	$\bar{u}_z$ [a]	$\bar{\sigma}_{xx}$ [b]	$\bar{\sigma}_{xz}$ [c]	DOF
Uniform Models							
TE1	TE1	TE1	2/2/2	1.5912	0.7506	0.5000	1098
TE2	TE2	TE2	3/3/3	1.5709	0.7507	0.5015	1647
TE3	TE3	TE3	4/4/4	1.5596	0.7721	0.7042	2196
TE4	TE4	TE4	5/5/5	1.5995	0.7632	0.7122	2745
Different models (Influence on u_y)							
TE4	TE0	TE4	5/1/5	1.5995	0.7632	0.7122	2013
Different models (Influence on u_z)							
TE4	TE0	TE0	5/1/1	1.6327	0.7695	0.7293	1281
TE4	TE0	TE1	5/1/2	1.6327	0.7695	0.7324	1464
TE4	TE0	TE2	5/1/3	1.5596	0.7722	0.7042	1647
TE4	TE0	TE3	5/1/4	1.5596	0.7722	0.7042	1830
Different models (Influence on u_x)							
TE0	TE0	TE4	1/1/5	0.2083	0.0161	0.4766	1281
TE1	TE0	TE4	2/1/5	1.5708	0.7501	0.5113	1464
TE2	TE0	TE4	3/1/5	1.5708	0.7501	0.5113	1647
TE3	TE0	TE4	4/1/5	1.5995	0.7632	0.7122	1830
Reduced Models							
Model 1			2/1/3	1.5995	0.7632	0.7122	1098
Model 2			2/1/2	1.5596	0.7721	0.7042	915

[a] Computed at $[a/2, b/2, 0]$.
[b] Computed at $[a/2, b/2, h/2]$.
[c] Computed at $[a, b/2, 0]$.

In the first rows of the tables, *uniform* models are presented. In the central rows, *different* models are studied. First, the influence on u_y is considered, and it is evident that the constant term is sufficient for both a/h. Therefore, TE0 is used hereinafter. Second, the study on the influence on u_z is taken into account. Third, the investigation into the influence on u_x shows that higher-order terms are needed. Finally, two *reduced theories* are also proposed to demonstrate how some terms are not necessary. Their explicit forms are given in the followings:

$$\text{Model 1:} \quad \begin{aligned} u_x &= z u_{x_1} + z^3 u_{x_2} \\ u_y &= u_{y_1} \\ u_z &= u_{z_1} + z^2 u_{z_2} + z^4 u_{z_3} \end{aligned} \tag{37}$$

Table 7
Simply-supported metallic plate under distributed constant pressure. Case $a/h = 100$.

Model u_x	Model u_y	Model u_z	$M_{u_x}/M_{u_y}/M_{u_z}$	$\bar{u}_z$ [a]	$\bar{\sigma}_{xx}$ [b]	$\bar{\sigma}_{xz}$ [c]	DOF
Uniform Models							
TE1	TE1	TE1	2/2/2	1.3822	0.7505	0.5000	1098
TE2	TE2	TE2	3/3/3	1.3822	0.7505	0.5418	1647
TE3	TE3	TE3	4/4/4	1.3822	0.7505	0.7496	2196
TE4	TE4	TE4	5/5/5	1.3822	0.7505	0.7496	2745
Different models (Influence on u_y)							
TE3	TE0	TE3	4/1/4	1.3822	0.7505	0.7496	1647
Different models (Influence on u_z)							
TE3	TE0	TE0	4/1/1	1.3823	0.7505	0.7498	1098
TE3	TE0	TE1	4/1/2	1.3823	0.7505	0.7498	1281
TE3	TE0	TE2	4/1/3	1.3822	0.7505	0.7496	1464
Different models (Influence on u_x)							
TE0	TE0	TE3	1/1/4	0.0003	0.0000	0.4999	1098
TE1	TE0	TE3	2/1/4	1.3822	0.7505	0.5418	1281
TE2	TE0	TE3	3/1/4	1.3822	0.7505	0.5418	1464
Reduced Models							
Model 1			2/1/3	1.3822	0.7505	0.7496	1098
Model 2			2/1/2	1.3822	0.7505	0.7496	915

[a] Computed at $[a/2, b/2, 0]$.
[b] Computed at $[a/2, b/2, h/2]$.
[c] Computed at $[a, b/2, 0]$.

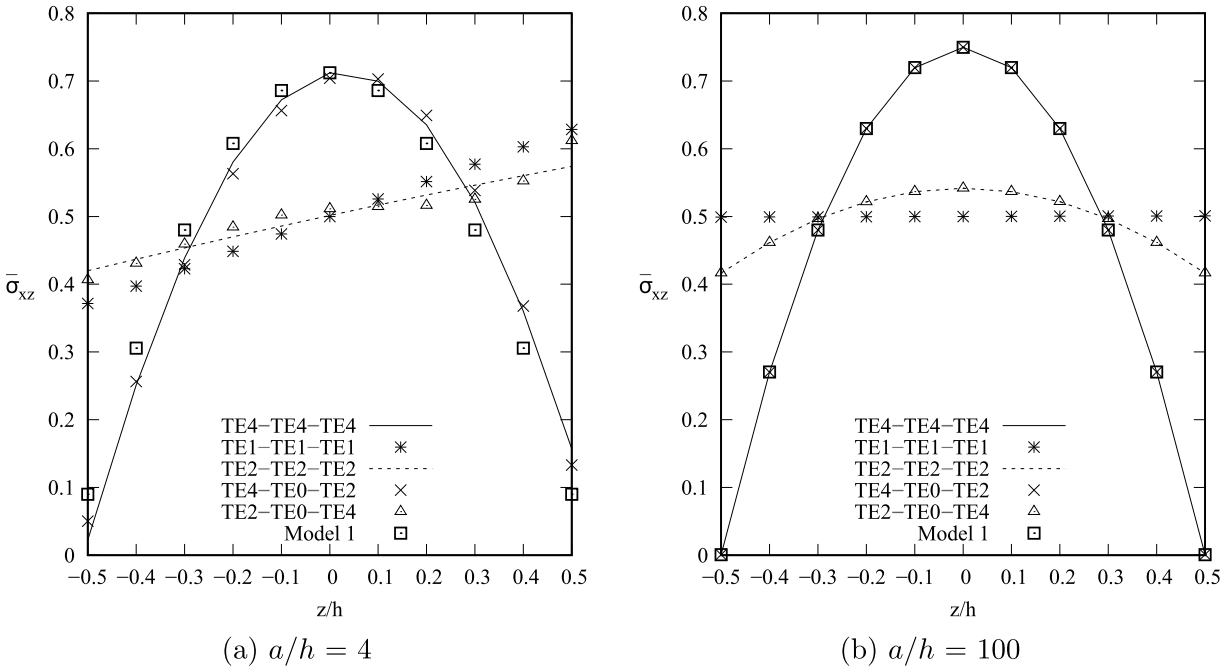

Fig. 21. Simply-supported metallic plate under distributed constant pressure. Thick (a) and thin (b) cases. Shear stresses, $\bar{\sigma}_{xz}$, evaluated in $[a, b/2, z]$.

$$\text{Model 2:} \quad \begin{aligned} u_x &= z u_{x_2} + z^3 u_{x_3} \\ u_y &= u_{y_1} \\ u_z &= u_{z_1} + z^2 u_{z_3} \end{aligned} \tag{38}$$

Figs. 21(a) and 21(b) graphically depict the trends of the shear stresses, $\bar{\sigma}_{xz}$, in the thick and thin cases, respectively, for some selected theories. Finally, Fig. 22 shows the relationship between length-to-thickness ratio, a/h, and the transverse displacement, $\bar{u}_z$, evaluated in $[a/2, b/2, 0]$. The reduced Model 1 is more precise than the TE2 model, even if the first has less DOF.

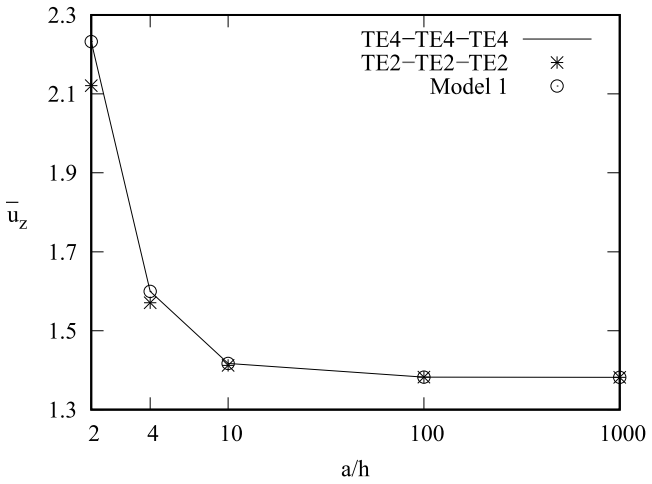

Fig. 22. Simply-supported metallic plate under distributed constant pressure. Relationship between length-to-thickness ratio, a/h, and the transverse displacement, $\bar{u}_z$ (evaluated in $[a/2, b/2, 0]$).

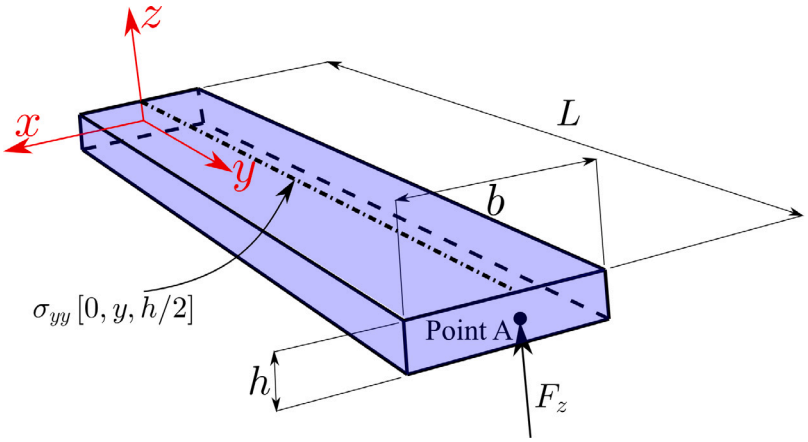

Fig. 23. Geometrical properties of Benchmark 3. Cantilever plate subjected to a point load. The study case is taken from [55,56].

The results leads to the following observations:

- The analysis remarks that higher-order terms are very important to reach results near to the complete model. However, only some terms are relevant for the determination of the outcomes. In particular, *reduced* Models 1 and 2 demonstrate how tailored theories may be very effective;
- The terms of the in-plane displacement variable u_x are the most significant in the solution. Conversely, the variable u_z is less critical;
- The length-to-thickness ratio significantly influences the behaviour of the outputs. Several terms are needed to obtain excellent results if the plate is thick, while few DOF are sufficient for the thin plate.

6.3. End-effects on a clamped plate

The third benchmark considered is a cantilevered plate. Ghazouani and El Fatmi [55] initially proposed this analysis, and it was further investigated by Carrera et al. [56]. Fig. 23 illustrates the geometrical properties of the structure. The height, h, is equal to 1 [m], and the ratio b/h is 0.5. The aspect ratio, L/h, is equal to six, where L is the length of the structure. The orthotropic material has the following properties: E_{11} = 206.80 [GPa], $E_{22} = E_{33}$ = 5.17 [GPa], $G_{12} = G_{13}$ = 3.10 [GPa], G_{23} = 2.55 [GPa], $\nu_{12} = \nu_{23} = \nu_{23}$ = 0.25. The plate is clamped at $y = 0$. A concentrated load is applied in the positive z-direction at Point A = $[0, L, 0]$, with a force of 1 [N]. The analysis focuses on the end effects caused by the boundary conditions. For the $L/h = 6$ case, the results are compared with a higher-order beam theory [55], a 3D FEM solution [55], and a 1D CUF-based solution [56]. The last solution adopts a fifth-order beam theory. Axial stresses, σ_{yy}, are evaluated along $[0, y, h/2]$, as illustrated in Fig. 23. For brevity,

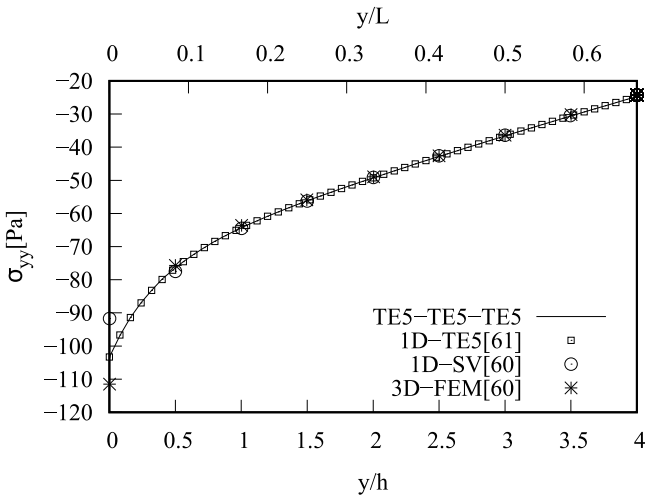

Fig. 24. End effects on a clamped plate for the reference solutions. The axial stresses are evaluated in $[0, y, h/2]$.

Table 8
End effects on a cantilevered plate. The axial stresses are evaluated in $[0, 0, h/2]$.

Model u_x	Model u_y	Model u_z	$M_{u_x}/M_{u_y}/M_{u_z}$	$-\sigma_{yy}$ [Pa]	err [%]	DOF
Uniform Models						
TE1	TE1	TE1	2/2/2	72.239	30.106	2730
TE2	TE2	TE2	3/3/3	72.256	30.088	4095
TE3	TE3	TE3	4/4/4	93.976	9.0734	5460
TE4	TE4	TE4	5/5/5	93.848	9.1979	6825
TE5	TE5	TE5	6/6/6	103.35	—[a]	8190
Different Models (Influence on u_x)						
TE0	TE5	TE5	1/6/6	103.15	0.1983	5915
TE1	TE5	TE5	2/6/6	103.32	0.0350	6370
TE2	TE5	TE5	3/6/6	103.32	0.0350	6825
Different Models (Influence on u_z)						
TE1	TE5	TE1	2/6/2	102.75	0.5885	4550
TE1	TE5	TE2	2/6/3	103.43	0.0750	5005
TE1	TE5	TE3	2/6/4	103.43	0.0750	5460
TE1	TE5	TE4	2/6/5	103.32	0.0350	5915
Different Models (Influence on u_y)						
TE1	TE1	TE2	2/2/3	72.256	30.088	3185
TE1	TE2	TE2	2/3/3	72.256	30.088	3640
TE1	TE3	TE2	2/4/3	93.902	9.1451	4095
TE1	TE4	TE2	2/5/3	93.902	9.1451	4550
Reduced Models						
Model 1			1/4/2	103.23	0.1181	3185
Model 2			1/4/1	102.41	0.9177	2730
Model 3			1/3/2	93.661	9.3777	2730
Model 4			1/3/2	103.23	0.1181	2730

[a] Taken as the reference solution.

the convergence analysis is not explicitly reported, and ninety MITC9 elements are used for all the analyses. Fig. 24 compares the literature solutions with the present uniform TE5 model. Since the results from TE5-TE5-TE5 are in good agreement, it is taken as the reference solution hereinafter.

The Poisson Locking correction is used if the maximum term of the u_z variable is linear.

Table 8 proposes several models. In-plane stresses are evaluated in $[0, 0, h/2]$. The error is presented in the sixth column. The following formula provides the relative error:

$$\text{err} = \left\| \frac{\sigma_{yy}\,(\text{TE5-TE5-TE5}) - \sigma_{yy}}{\sigma_{yy}\,(\text{TE5-TE5-TE5})} \right\| \times 100 \tag{39}$$

In the first rows, the *uniform* models are analysed. *Different* models are studied in a systematic way. First, the influence on u_x is considered. Second, the expansions TE1 and TE5 are fixed for the variables u_x and u_y, respectively, studying the importance of the variable u_z Third, the influence on u_y is studied. In the last rows, four *reduced* theories are taken into account. Their mathematical models are written below:

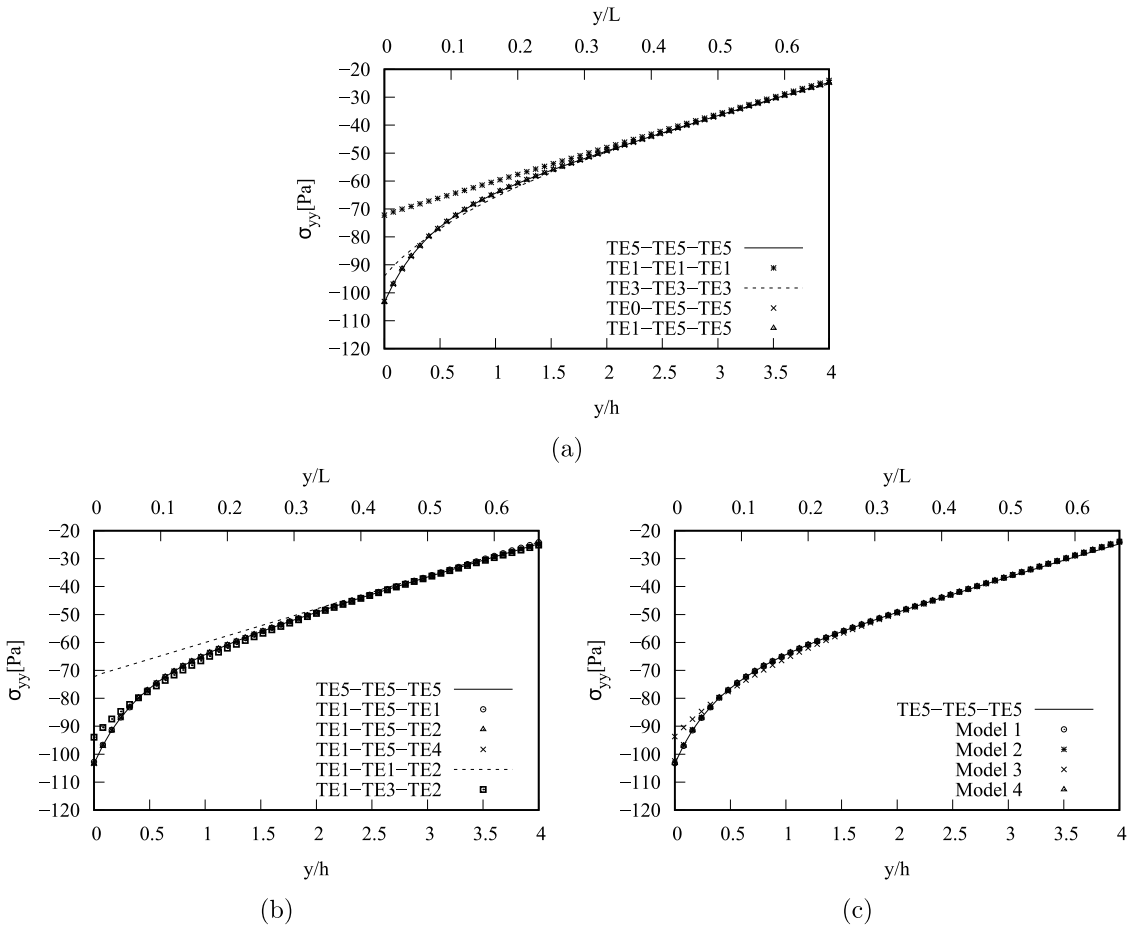

Fig. 25. End effects on a cantilevered plate for the present models. The axial stresses, σ_{yy}, are evaluated in $[0, y, h/2]$.

$$\text{Model 1:}\quad \begin{aligned} u_x &= u_{x_1} \\ u_y &= u_{y_1} + z u_{y_2} + z^3 u_{y_3} + z^5 u_{y_4} \\ u_z &= u_{z_1} + z^2 u_{z_2} \end{aligned} \tag{40}$$

$$\text{Model 2:}\quad \begin{aligned} u_x &= u_{x_1} \\ u_y &= u_{y_1} + z u_{y_2} + z^3 u_{y_3} + z^5 u_{y_4} \\ u_z &= u_{z_1} \end{aligned} \tag{41}$$

$$\text{Model 3:}\quad \begin{aligned} u_x &= u_{x_1} \\ u_y &= u_{y_1} + z u_{y_2} + z^3 u_{y_3} \\ u_z &= u_{z_1} \end{aligned} \tag{42}$$

$$\text{Model 4:}\quad \begin{aligned} u_x &= u_{x_1} \\ u_y &= z u_{y_1} + z^3 u_{y_2} + z^5 u_{y_3} \\ u_z &= u_{z_1} + z^2 u_{z_2} \end{aligned} \tag{43}$$

Fig. 25 graphically presents the trends of the stresses along the line $[0, y, h/2]$. In particular, Figs. 25(a) and 25(b) deal with the *uniform* and *different* models. Figs. 25(c) focuses on the *reduced* theories.

Some important observations can be made based on the results:

- It is worthy noting that the end effects are relevant in a restricted areas. To this end, the necessity of higher-order terms is pivotal to underline the trend of the stresses, σ_{yy}, near the clamped area;

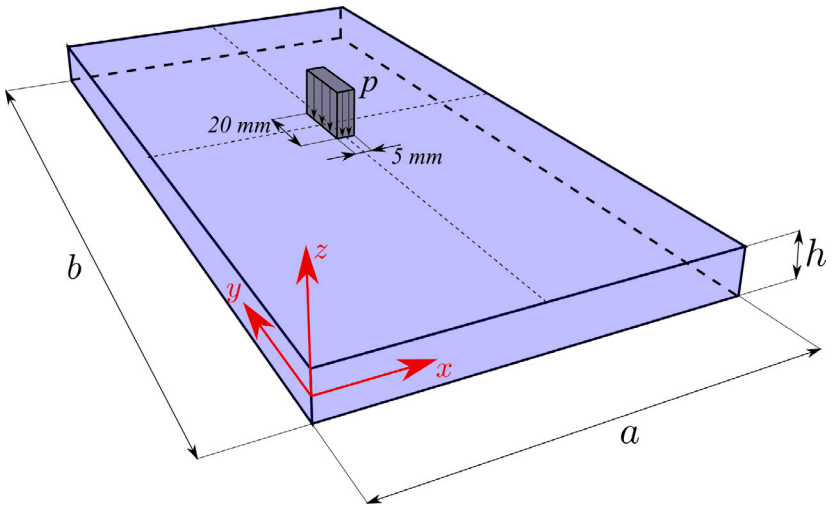

Fig. 26. Geometrical properties of the Benchmark 4. Simply-supported isotropic plate loaded by a localized constant pressure.

- The problem exhibits less sensitivity to the model for u_x, where only the constant term is needed. On the other hand, to attain accurate results, it is essential to retain more terms in models for u_y and u_z. These considerations are well illustrated when the *reduced* models are adopted.

6.4. Isotropic plate loaded by localized distribution of pressure

A metallic plate is analysed as the final example, presented as a benchmark for the first time in this work. The geometric and loading conditions are described in Fig. 26. The plate is subjected to a constant pressure of 1 [MPa], applied within a rectangular zone located at the plate centre with dimensions of 5×20 [mm^2]. The plate's geometric parameters are $a = 100$ [mm], $b = 200$ [mm], and $h = 12$ [mm]. The material properties are defined as follows: E = 70 [GPa], G = 26 [GPa], $\nu = 0.3$. The plate is simply supported along all four edges. Thanks to the symmetry of structure and loading conditions, a quarter of the plate is taken into account. The study evaluates transverse displacements, u_z, and in-plane stresses, σ_{xx}. For comparison purposes, they are non-dimensionalized form as follows:

$$\overline{u}_z = \frac{100\ E\ u_z}{p\left(\frac{b}{h}\right)^2 h} \qquad \overline{\sigma}_{xx} = \frac{100\ \sigma_{xx}}{p\left(\frac{b}{h}\right)^2} \tag{44}$$

A non-uniform mesh grid of 38×54 elements is employed for all analyses. Due to space constraints, the convergence analysis is omitted.

Table 9 shows the transverse displacements, u_z, and the in-plane stresses, σ_{xx}, calculated in $[a/2, b/2, h/2]$. The complete theory TE4-TE4-TE4 is taken as the reference solution. For a complete comparison, TE1-TE1-TE1 is studied by corrected and non-corrected strategy. In this case uniform and reduced models are taken into account. The explicit mathematical expressions of the reduced theories are given below:

$$\text{Model 1:} \quad \begin{aligned} u_x &= u_{x_1} + z u_{x_2} \\ u_y &= u_{y_1} + z u_{y_2} \\ u_z &= u_{z_1} + z u_{z_2} + z^2 u_{z_3} \end{aligned} \tag{45}$$

$$\text{Model 2:} \quad \begin{aligned} u_x &= u_{x_1} + z u_{x_2} + z^2 u_{x_3} + z^4 u_{x_4} \\ u_y &= u_{y_1} + z u_{y_2} \\ u_z &= u_{z_1} + z u_{z_2} + z^2 u_{z_3} \end{aligned} \tag{46}$$

$$\text{Model 3:} \quad \begin{aligned} u_x &= u_{x_1} + z u_{x_2} + z^2 u_{x_3} + z^4 u_{x_4} \\ u_y &= u_{y_1} + z u_{y_2} + z^2 u_{y_3} + z^3 u_{y_4} \\ u_z &= u_{z_1} + z u_{z_2} + z^2 u_{z_3} \end{aligned} \tag{47}$$

Finally, Fig. 27 graphically presents the trends of the transverse displacements along the line $[x, b/2, h/2]$. In particular, Figs. 27(a) and 27(b) show the results for the uniform and the reduced models, respectively. Magnifiers are illustrated near the loading part. On the other hand, Fig. 28 illustrates the in-plane stresses along the same line.

The main conclusions may be drawn as follows:

Table 9
Isotropic plate loaded by localized distribution of pressure. Transverse displacements are evaluated in $[a/2, b/2, h/2]$.

Model u_x	Model u_y	Model u_z	$M_{u_x}/M_{u_y}/M_{u_z}$	$-\bar{u}_z$	$-\bar{\sigma}_{xx}$	DOF
Uniform Models						
TE1	TE1	TE1$^{\text{no Corr}}$	2/2/2	2.856	0.517	50358
TE1	TE1	TE1$^{\text{Corr}}$	2/2/2	3.428	0.491	50358
TE2	TE2	TE2	3/3/3	3.376	0.592	75537
TE3	TE3	TE3	4/4/4	3.424	0.708	100716
TE4	TE4	TE4	5/5/5	3.427	0.725	125895[a]
Reduced Models						
Model 1			2/2/3	3.368	0.497	58571
Model 2			4/2/3	3.407	0.713	75537
Model 3			4/4/3	3.424	0.727	92323

[a] Taken as the reference solution.

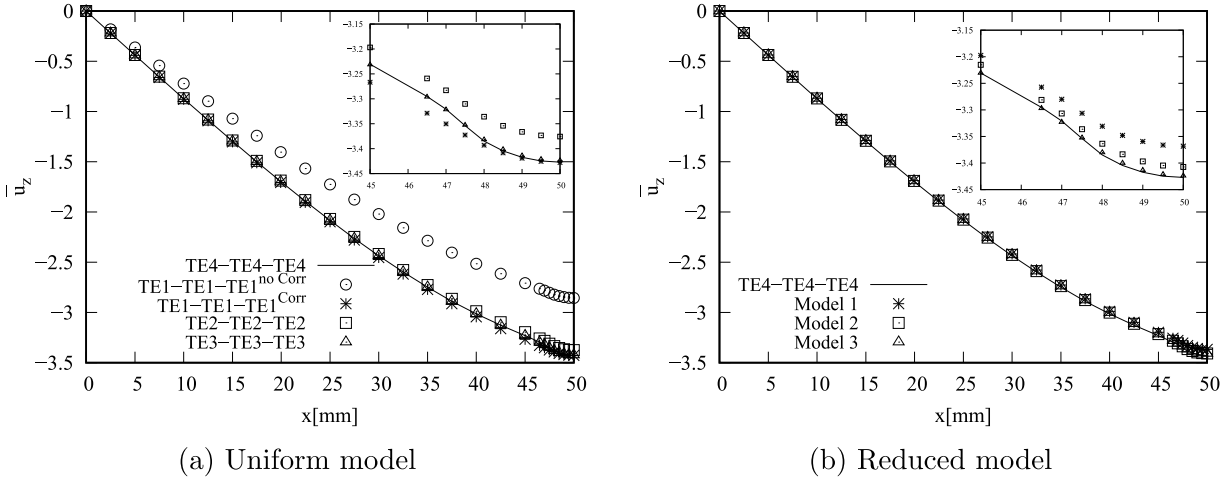

Fig. 27. Isotropic plate loaded by localized distribution of pressure. Transverse displacements are evaluated along $[x, b/2, h/2]$.

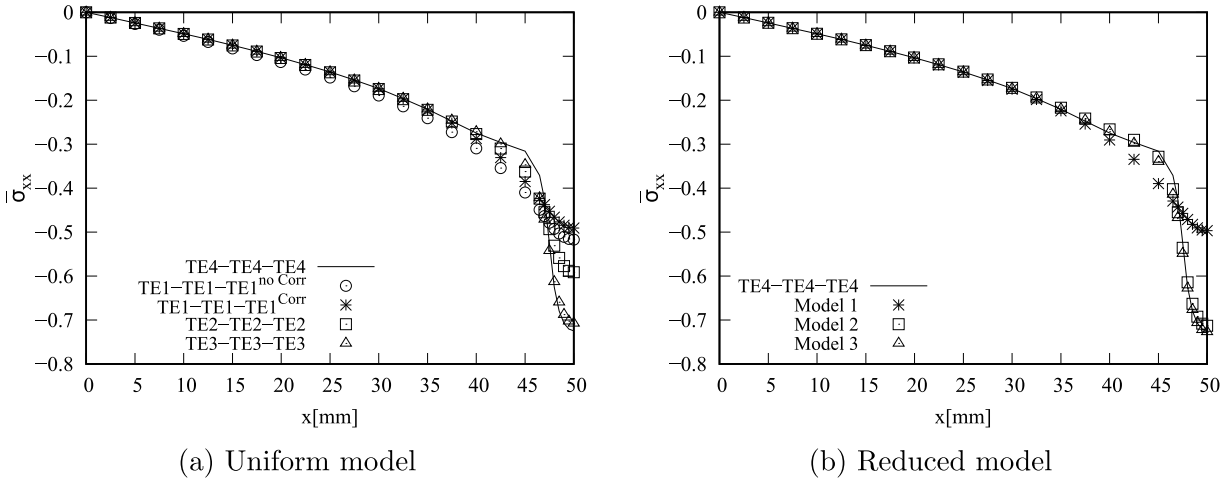

Fig. 28. Isotropic plate loaded by localized distribution of pressure. In-plane stresses, σ_{xx}, are evaluated along $[x, b/2, h/2]$.

- Higher-order terms are needed to study the behaviour in the vicinity of the loaded area. This is particularly true when the in-plane stresses are considered;
- The corrected TE1-TE1-TE1 model is able to approach the best solution when the displacements are analysed;
- When studying the stresses, the in-plane displacement variable, u_x, greatly influences the results;
- The example shows the possibility to use only relevant terms to arrive to interesting results.

7. Conclusions

This paper introduces a novel approach to constructing plate theories within the framework of the Carrera Unified Formulation (CUF). This approach allows for the development of dedicated structural theories for each displacement variable. In this way, tailored two-dimensional finite elements can be created. Additionally, the Mixed Interpolation of Tensorial Components method is incorporated into the framework. Four benchmarks are studied to assess the method, considering literature and CUF-based closed-form solutions as references in some cases. The analysis includes structures with varying thickness and loading conditions, considering both clamped and simply-supported plates.

To summarize the results, Table 10 presents noteworthy outcomes for the three benchmarks. Graphical trends, along with the degrees of freedom, are illustrated for comparison purposes. Shear stresses, σ_{xz}, are displayed for the first two benchmarks, considering thick cases. In-plane stresses, σ_{yy}, are analysed in the clamped plate case. Based on the results obtained throughout the paper, the following conclusions can be drawn:

- Significant reduction in computational costs is achievable by selectively utilizing only the most relevant terms within the structural theories;
- The choice of the appropriate kinematics model depends on the plate geometry, specific loads, and boundary conditions;
- The use of the MITC method is indeed of paramount importance if thin structures are considered;
- The number of effective variables is highly dependent on the nature of the problem under consideration.

Proposal for determining the best computational model. This paper marks the first stage in devising a method to systematically identify the most appropriate theories for plate formulation. Future companion papers will detail additional steps in this process. These steps can be summarized as follows:

(I) The current paper lays out the theoretical groundwork for developing simplified models. At present, identical models are being employed for all the FE of the plates;
(II) A technique is utilized to analyse the plate thickness-wise, where each thickness-line is approximated by a distinct structural theory. For instance, the Node Dependent Kinematics (NDK) approach can be applied utilizing CUF capabilities [57]. As implied by its name, NDK enables the selection of the expansion theory for each FE node. Consequently, the reduced models and NDK will complement each other in a synergic way;
(III) Analysing and categorizing the proposed theories can be achieved through the AAM. Initially, the AAM is constructed solely for models that are uniform across the plate. Subsequently, the AAM is integrated with the NDK. Previous efforts in the CUF literature have explored this direction [58] The aim is to compare all combinations and visually represent them in a diagram;
(IV) To systematically analyse this information and reduce analysis time, innovative techniques such as data mining and machine learning can be employed. As the number of theory combinations can be substantial, dealing with complex structures might become unfeasible. For instance, genetic algorithms and neural networks have been utilized in CUF literature [43,58] for determining the best theories;
(V) The final objective is to establish a database for training a neural network. This tool would subsequently assist in determining the optimal model based on specified accuracy requirements, considering factors such as boundary conditions, loads, materials, and other pertinent characteristics.

All these steps will be proposed and integrated into a unified framework by leveraging the capabilities offered by CUF.

Furthermore, other possibilities are under development. Currently, a paper on shell structures is in preparation. Additionally, applying the variable structural approximations presented here to composite plates holds significant potential. Finally, exploring the application to multi-field analyses could be very promising.

CRediT authorship contribution statement

E. Carrera: Writing – review & editing, Supervision, Methodology, Funding acquisition, Conceptualization. **D. Scano:** Writing – original draft, Visualization, Software, Methodology, Investigation, Formal analysis, Data curation, Conceptualization. **E. Zappino:** Writing – review & editing, Validation, Supervision, Software, Data curation, Conceptualization.

Declaration of competing interest

The authors declare that they have no known competing financial interests or personal relationships that could have appeared to influence the work reported in this paper.

Table 10
Some results obtained during the present analyses for different cases.

Bi-sinusoidal pressure for square plate. Case $a/h = 4$.

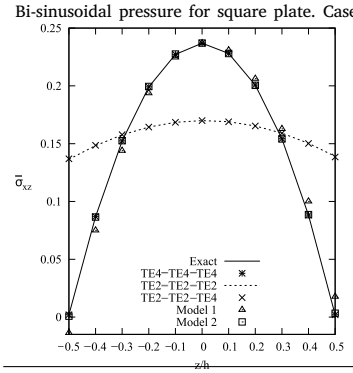

Theory	DOF
Exact	—
TE4-TE4-TE4	25125
TE2-TE2-TE2	15129
TE2-TE2-TE4	18491
Model 1, Eq. (33)	16810
Model 2, Eq. (34)	20172

Constant pressure for a rectangular plate. Case $a/h = 4$.

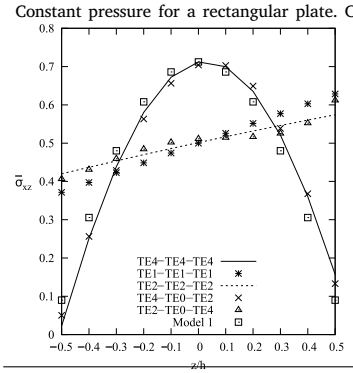

Theory	DOF
TE4-TE4-TE4	2745
TE1-TE1-TE1	1098
TE4-TE0-TE2	1647
TE2-TE0-TE4	1647
Model 1, Eq. (37)	1098

End-Effects on a clamped plate.

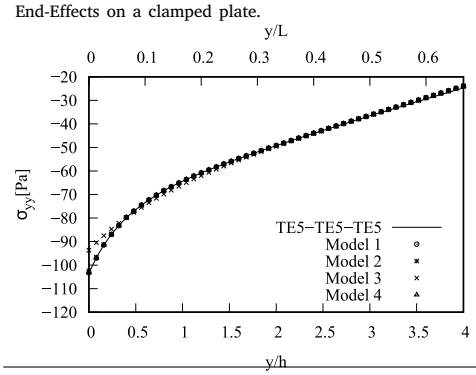

Theory	DOF
TE5-TE5-TE5	8190
Model 1, Eq. (40)	3185
Model 2, Eq. (41)	2730
Model 3, Eq. (42)	2730
Model 4, Eq. (43)	2730

Isotropic plate loaded by localized distribution of pressure.

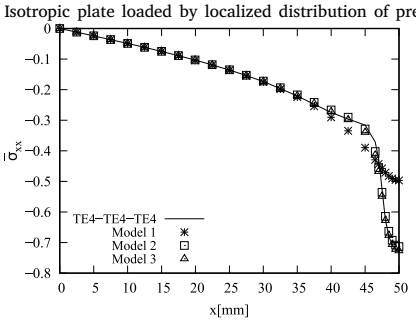

Theory	DOF
TE4-TE4-TE4	125895
Model 1, Eq. (45)	58571
Model 2, Eq. (46)	75537
Model 3, Eq. (47)	92323

Appendix. Explicit expression of the nine fundamental nuclei

$$
\begin{aligned}
K_{u_x u_x s\tau ji} = {} & C_{11} N_{j,x}^{n1} N_{i,x}^{m1} \int_{\Omega} N_{n1} N_{m1} \mathrm{d}x\mathrm{d}y \int_{A} F_{u_x s} F_{u_x \tau} \mathrm{d}z \\
& + C_{55} N_{j}^{n1} N_{i}^{m1} \int_{\Omega} N_{n1} N_{m1} \mathrm{d}x\mathrm{d}y \int_{A} F_{u_x s,z} F_{u_x \tau,z} \mathrm{d}z \\
& + C_{66} N_{j,y}^{n3} N_{i,y}^{m3} \int_{\Omega} N_{n3} N_{m3} \mathrm{d}x\mathrm{d}y \int_{A} F_{u_x s} F_{u_x \tau} \mathrm{d}z
\end{aligned} \tag{48}
$$

$$
\begin{aligned}
K_{u_x u_y s\tau ji} = {} & C_{12} N_{j,y}^{n2} N_{i,x}^{m1} \int_{\Omega} N_{n2} N_{m1} \mathrm{d}x\mathrm{d}y \int_{A} F_{u_x s} F_{u_y \tau} \mathrm{d}z \\
& + C_{66} N_{j,x}^{n3} N_{i,y}^{m3} \int_{\Omega} N_{n3} N_{m3} \mathrm{d}x\mathrm{d}y \int_{A} F_{u_x s} F_{u_y \tau} \mathrm{d}z
\end{aligned} \tag{49}
$$

$$
\begin{aligned}
K_{u_x u_z s\tau ji} = {} & C_{13} N_{i,x}^{m1} \int_{\Omega} N_{j} N_{m1} \mathrm{d}x\mathrm{d}y \int_{A} F_{u_x s,z} F_{u_z \tau} \mathrm{d}z \\
& + C_{55} N_{j,x}^{n1} N_{i}^{m1} \int_{\Omega} N_{n1} N_{m1} \mathrm{d}x\mathrm{d}y \int_{A} F_{u_x s} F_{u_z \tau,z} \mathrm{d}z
\end{aligned} \tag{50}
$$

$$
\begin{aligned}
K_{u_y u_x s\tau ji} = {} & C_{12} N_{j,x}^{n1} N_{i,y}^{m2} \int_{\Omega} N_{n1} N_{m2} \mathrm{d}x\mathrm{d}y \int_{A} F_{u_y s} F_{u_x \tau} \mathrm{d}z \\
& + C_{66} N_{j,y}^{n3} N_{i,x}^{m3} \int_{\Omega} N_{n3} N_{m3} \mathrm{d}x\mathrm{d}y \int_{A} F_{u_y s} F_{u_x \tau} \mathrm{d}z
\end{aligned} \tag{51}
$$

$$
\begin{aligned}
K_{u_y u_y s\tau ji} = {} & C_{22} N_{j,y}^{n2} N_{i,y}^{m2} \int_{\Omega} N_{n2} N_{m2} \mathrm{d}x\mathrm{d}y \int_{A} F_{u_y s} F_{u_y \tau} \mathrm{d}z \\
& + C_{44} N_{j}^{n2} N_{i}^{m2} \int_{\Omega} N_{n2} N_{m2} \mathrm{d}x\mathrm{d}y \int_{A} F_{u_y s,z} F_{u_y \tau,z} \mathrm{d}z \\
& + C_{66} N_{j,x}^{n3} N_{i,x}^{m3} \int_{\Omega} N_{n3} N_{m3} \mathrm{d}x\mathrm{d}y \int_{A} F_{u_y s} F_{u_y \tau} \mathrm{d}z
\end{aligned} \tag{52}
$$

$$
\begin{aligned}
K_{u_y u_z s\tau ji} = {} & C_{23} N_{i,y}^{m2} \int_{\Omega} N_{j} N_{m2} \mathrm{d}x\mathrm{d}y \int_{A} F_{u_y s,z} F_{u_z \tau} \mathrm{d}z \\
& + C_{44} N_{j,y}^{n2} N_{i}^{m2} \int_{\Omega} N_{n2} N_{m2} \mathrm{d}x\mathrm{d}y \int_{A} F_{u_y s} F_{u_z \tau,z} \mathrm{d}z
\end{aligned} \tag{53}
$$

$$
\begin{aligned}
K_{u_z u_x s\tau ji} = {} & C_{13} N_{j,x}^{n1} \int_{\Omega} N_{n1} N_{i} \mathrm{d}x\mathrm{d}y \int_{A} F_{u_z s} F_{u_x \tau,z} \mathrm{d}z \\
& + C_{55} N_{j}^{n1} N_{i,x}^{m1} \int_{\Omega} N_{n1} N_{m1} \mathrm{d}x\mathrm{d}y \int_{A} F_{u_z s,z} F_{u_x \tau} \mathrm{d}z
\end{aligned} \tag{54}
$$

$$
\begin{aligned}
K_{u_z u_y s\tau ji} = {} & C_{23} N_{j,y}^{n2} \int_{\Omega} N_{n2} N_{i} \mathrm{d}x\mathrm{d}y \int_{A} F_{u_z s} F_{u_y \tau,z} \mathrm{d}z \\
& + C_{44} N_{j}^{n2} N_{i,y}^{m2} \int_{\Omega} N_{n2} N_{m2} \mathrm{d}x\mathrm{d}y \int_{A} F_{u_z s,z} F_{u_y \tau} \mathrm{d}z
\end{aligned} \tag{55}
$$

$$
\begin{aligned}
K_{u_z u_z s\tau ji} = {} & C_{33} \int_{\Omega} N_{j} N_{i} \mathrm{d}x\mathrm{d}y \int_{A} F_{u_z s,z} F_{u_z \tau,z} \mathrm{d}z \\
& + C_{44} N_{j,y}^{n2} N_{i,y}^{m2} \int_{\Omega} N_{n2} N_{m2} \mathrm{d}x\mathrm{d}y \int_{A} F_{u_z s} F_{u_z \tau} \mathrm{d}z \\
& + C_{55} N_{j,x}^{n1} N_{i,x}^{m1} \int_{\Omega} N_{n1} N_{m1} \mathrm{d}x\mathrm{d}y \int_{A} F_{u_z s} F_{u_z \tau} \mathrm{d}z
\end{aligned} \tag{56}
$$

Data availability

Data will be made available on request.

References

[1] E. Zappino, E. Carrera, Multidimensional model for the stress analysis of reinforced shell structures, AIAA J. 56 (4) (2018) 1647–1661.
[2] E. Carrera, L. Demasi, Classical and advanced multilayered plate elements based upon PVD and RMVT. Part 1: Derivation of finite element matrices, Internat. J. Numer. Methods Engrg. 55 (2) (2002) 191–231.
[3] G. Kirchhoff, Über das Gleichgewicht und die Bewegung einer elastischen Scheibe, J. Reine Angew. Math. 40 (1850) 51–88.
[4] E. Reissner, The effect of transverse shear deformation on the bending of elastic plates, J. Appl. Mech. 12 (1945) 69–77.
[5] R.D. Mindlin, Influence of rotary inertia and shear on flexural motions of isotropic, elastic plates, J. Appl. Mech.-Trans. ASME 18 (1951) 31–38.
[6] J.H. Argyris, Matrix displacement analysis of plates and shells, Prolegomena to a general theory, Part I, Ingeniur-Archiv 35 (1966) 102–142.
[7] C.W. Pryor, R.M. Baeker, A finite-element analysis including transverse shear effects for applications to laminated plates, AIAA J. 9 (5) (1971) 912–917.
[8] L. Leonetti, M. Aristodemo, A composite mixed finite element model for plane structural problems, Finite Elem. Anal. Des. 94 (2015) 33–46.
[9] D. Ribari, G. Jelenic, Higher-order linked interpolation in quadrilateral thick plate finite elements, Finite Elem. Anal. Des. 51 (2012) 67–80.
[10] K.J. Bathe, Finite Element Procedure, Prentice hall, Upper Saddle River, New Jersey, USA, 1996.
[11] J.H. Argyris, Matrix analysis of three-dimensional elastic media - small and large displacements, AIAA J. 3 (1) (1965) 45–51.
[12] K.S. Surana, Transition finite elements for three-dimensional stress analysis, Internat. J. Numer. Methods Engrg. 15 (7) (1980) 991–1020.
[13] K.S. Surana, Geometrically non-linear formulation for the three dimensional solid-shell transition finite elements, Comput. Struct. 15 (5) (1982) 549–566.
[14] C.G. Dávila, Solid-to-shell transition elements for the computation of interlaminar stresses, Comput. Syst. Eng. 5 (2) (1994) 193–202.
[15] P.J. Blanco, R.A. Feijóo, S.A. Urquiza, A variational approach for coupling kinematically incompatible structural models, Comput. Methods Appl. Mech. Engrg. 197 (17) (2008) 1577–1602.
[16] A.K. Noor, Global-local methodologies and their application to nonlinear analysis, Finite Elem. Anal. Des. 2 (4) (1986) 333–346.
[17] J.N. Reddy, Mechanics of Laminated Composite Plates and Shells: Theory and Analysis, CRC Press, New York, USA, 1997.
[18] J.N. Reddy, D.H. Robbins, Theories and computational models for composite laminates, Appl. Mech. Rev. 47 (6) (1994) 147–169.
[19] E. Carrera, Developments, ideas, and evaluations based upon Reissner's Mixed Variational Theorem in the modeling of multilayered plates and shells, Appl. Mech. Rev. 54 (4) (2001) 301–329.
[20] K. Washizu, Variational Methods in Elasticity and Plasticity, Pergamon, Oxford, United Kingdom, 1968.
[21] T. Kant, D.R.J. Owen, O.C. Zienkiewicz, A refined higher-order C° plate bending element, Comput. Struct. 15 (2) (1982) 177–183.
[22] T. Kant, J.R. Kommineni, Large amplitude free vibration analysis of cross-ply composite and sandwich laminates with a refined theory and C° finite elements, Comput. Struct. 50 (1) (1994) 123–134.
[23] J.N. Reddy, An evaluation of equivalent-single-layer and layerwise theories of composite laminates, Compos. Struct. 25 (1) (1993) 21–35.
[24] K. Swaminathan, S.S. Patil, Analytical solutions using a higher order refined computational model with 12 degrees of freedom for the free vibration analysis of antisymmetric angle-ply plates, Compos. Struct. 82 (2) (2008) 209–216.
[25] T. Kant, K. Swaminathan, Free vibration of isotropic, orthotropic, and multilayer plates based on higher order refined theories, J. Sound Vib. 241 (2) (2001) 319–327.
[26] T. Kant, B.S. Manjunatha, An unsymmetric FRC laminate C° finite element model with 12 degrees of freedom per node, Eng. Comput. 5 (4) (1988) 300–308.
[27] B.N. Pandya, T. Kant, Finite element analysis of laminated composite plates using a higher-order displacement model, Compos. Sci. Technol. 32 (2) (1988) 137–155.
[28] J.N. Reddy, A simple higher-order theory for laminated composite plates, J. Appl. Mech. 51 (1984) 745–752.
[29] N.R. Senthilnathan, S.P. Lim, K.H. Lee, S.T. Chow, Buckling of Shear-Deformable Plates, AIAA J. 25 (9) (1987) 1268–1271.
[30] J.M. Whitney, N.J. Pagano, Shear Deformation in Heterogeneous Anisotropic Plates, J. Appl. Mech. 37 (4) (1970) 1031–1036.
[31] E. Carrera, A. Pagani, F. Zangallo, Comparison of various 1D, 2D and 3D FE models for the analysis of thin-walled box with transverse ribs subjected to load factors, Finite Elem. Anal. Des. 95 (2015) 1–11.
[32] A. Robaldo, E. Carrera, A. Benjeddou, Unified formulation for finite element thermoelastic analysis of multilayered anisotropic composite plates, J. Therm. Stresses 28 (10) (2005) 1031–1065.
[33] D. Ballhause, M. d'Ottavio, B. Kröplin, E. Carrera, A unified formulation to assess multilayered theories for piezoelectric plates, Comput. Struct. 83 (15–16) (2005) 1217–1235.
[34] E. Carrera, Theories and Finite Elements for Multilayered Plates and Shells: A Unified compact formulation with numerical assessment and benchmarking, Arch. Comput. Methods Eng. 10 (2003) 215–296.
[35] A. Pagani, E. Carrera, D. Scano, R. Augello, Finite elements based on Jacobi shape functions for the analysis of beams, plates and shells, Internat. J. Numer. Methods Engrg. 124 (20) (2023) 4490–4519.
[36] A.L. Gol'denveizer, Theory of Elastic Thin Shells, Pergamon Press, Oxford, United Kingdom, 1961.
[37] P. Cicala, Systematic Approximation Approach to Linear Shell Theory, Levrotto e Bella, Turin, Italy, 1965.
[38] L.A. Aghalovyan, M.L. Aghalovyan, On Asymptotic Theory of Beams, Plates and Shells, Curved Layer. Struct. 3 (1) (2016).
[39] V.L. Berdichevsky, An asymptotic theory of sandwich plates, Internat. J. Engrg. Sci. 48 (3) (2010) 383–404.
[40] E. Carrera, M. Petrolo, Guidelines and Recommendations to Construct Theories for Metallic and Composite Plates, AIAA J. 48 (12) (2010) 2852–2866.
[41] E. Reissner, On transverse bending of plates, including the effect of transverse shear deformation, Int. J. Solids Struct. 11 (5) (1975) 569–573.
[42] E. Carrera, D. Scano, E. Zappino, One-dimensional Finite Elements with Arbitrary Cross-Sectional Displacement Fields, 2024, Under review.
[43] M. Petrolo, A. Lamberti, F. Miglioretti, Best theory diagram for metallic and laminated composite plates, Mech. Adv. Mater. Struct. 23 (9) (2016) 1114–1130.
[44] M. Petrolo, A. Lamberti, Axiomatic/asymptotic analysis of refined layer-wise theories for composite and sandwich plates, Mech. Adv. Mater. Struct. 23 (1) (2016) 28–42.
[45] M. Petrolo, E. Carrera, Best theory diagrams for multilayered structures via shell finite elements, Adv. Model. Simul. Eng. Sci. 6 (4) (2019) 1–23.
[46] L. Demasi, ∞^3 hierarchy plate theories for thick and thin composite plates: The generalized unified formulation, Compos. Struct. 84 (3) (2008) 256–270.
[47] L. Demasi, Partially Layer Wise advanced Zig Zag and HSDT models based on the Generalized Unified Formulation, Eng. Struct. 53 (2013) 63–91.
[48] K.J. Bathe, E.N. Dvorkin, A formulation of general shell elements—the use of mixed interpolation of tensorial components, Internat. J. Numer. Methods Engrg. 22 (1986) 697–722.
[49] M.L. Bucalem, K.J. Bathe, Higher-order MITC general shell elements, Internat. J. Numer. Methods Engrg. 36 (21) (1993) 3729–3754.
[50] M. Cinefra, E. Carrera, Shell finite elements with different through-the-thickness kinematics for the linear analysis of cylindrical multilayered structures, Internat. J. Numer. Methods Engrg. 93 (2) (2013) 160–182.
[51] E. Carrera, M. Cinefra, M. Petrolo, E. Zappino, Finite Element Analysis of Structures Through Unified Formulation, John Wiley & Sons, 2014.
[52] K.H. Lo, R.M. Christensen, E.M. Wu, A High-Order Theory of Plate Deformation—Part 1: Homogeneous Plates, J. Appl. Mech. 44 (4) (1977) 663–668.
[53] B.S. Manjunatha, T. Kant, Different numerical techniques for the estimation of multiaxial stresses in symmetric/unsymmetric composite and sandwich beams with refined theories, J. Reinf. Plast. Compos. 12 (1) (1993) 2–37.
[54] K.J. Bathe, F. Brezzi, S.W. Cho, The MITC7 and MITC9 plate bending elements, Comput. Struct. 32 (3) (1989) 797–814.

[55] N. Ghazouani, R. El Fatmi, Higher order composite beam theory built on Saint-Venant's solution. Part II: Built-in effects influence on the behavior of end-loaded cantilever beams, Compos. Struct. 93 (2) (2011) 567–581.
[56] E. Carrera, M. Petrolo, E. Zappino, Performance of CUF approach to analyze the structural behavior of slender bodies, J. Struct. Eng. 138 (2) (2012) 285–297.
[57] E. Zappino, G. Li, A. Pagani, E. Carrera, A.G. de Miguel, Use of higher-order Legendre polynomials for multilayered plate elements with node-dependent kinematics, Compos. Struct. 202 (2018) 222–232, Special issue dedicated to Ian Marshall.
[58] M. Petrolo, E. Carrera, Best spatial distributions of shell kinematics over 2D meshes for free vibration analyses, Aerotecnica Missili & Spazio 99 (2020) 217–232.